Spectral Analysis on Transport Budgets of Turbulent Heat Fluxes in Plane Couette Turbulence

Takuya Kawata [1,*] and **Takahiro Tsukahara** [2]

1 Department of Mechanical Engineering, Keio University, Hiyoshi 3-14-1, Yokohama 223-8522, Japan
2 Department of Mechanical Engineering, Tokyo University of Science, Yamazaki 2641, Noda 278-8510, Japan; tsuka@rs.tus.ac.jp
* Correspondence: kawata@keio.jp

Abstract: In recent years, scale-by-scale energy transport in wall turbulence has been intensively studied, and the complex spatial and interscale transfer of turbulent energy has been investigated. As the enhancement of heat transfer is one of the most important aspects of turbulence from an engineering perspective, it is also important to study how turbulent heat fluxes are transported in space and in scale by nonlinear multi-scale interactions in wall turbulence as well as turbulent energy. In the present study, the spectral transport budgets of turbulent heat fluxes are investigated based on direct numerical simulation data of a turbulent plane Couette flow with a passive scalar heat transfer. The transport budgets of spanwise spectra of temperature fluctuation and velocity-temperature correlations are investigated in detail in comparison to those of the corresponding Reynolds stress spectra. The similarity and difference between those scale-by-scale transports are discussed, with a particular focus on the roles of interscale transport and spatial turbulent diffusion. As a result, it is found that the spectral transport of the temperature-related statistics is quite similar to those of the Reynolds stresses, and in particular, the inverse interscale transfer is commonly observed throughout the channel in both transport of the Reynolds shear stress and wall-normal turbulent heat flux.

Keywords: wall-bounded turbulent flow; turbulent heat transfer; multi-scale interaction; turbulent energy transport; direct numerical simulation

1. Introduction

Analysing the budgets of the Reynolds stress transport equation is a useful tool for investigating turbulence transport phenomena as it shows quantitatively where and how much turbulence is produced from the mean flow, redistributed among different velocity components by the effect of pressure, dissipated into heat by viscosity, etc. A particularly interesting feature is that the budget includes spatial transport (or diffusion) terms, which do not lead to total energy gain/loss of turbulent energy across the flow field but represent spatial transports by different effects, namely, advection by the mean flow and diffusion by turbulence, pressure fluctuation and viscosity. Similarly to the Reynolds stress transport equation, one can derive the transport equations of passive-scalar fluxes, and one of the most engineering-relevant features of turbulence to enhance the spatial transport of heat and mass may be expressed by the turbulent diffusion terms in these transport equations.

The budget analysis of the Reynolds stress (or turbulent kinetic energy) transport equation has recently been extended to scale-by-scale budget analysis, where the transport equation is decomposed into large- and small-scale parts (e.g., Refs. [1–5]) or the spectral transport equation [6–8] is derived. Similar analysis of the energy transport at each scale is also possible based on the transport equations of two-point correlation quantities, such as the second-order structure function (e.g., Refs. [9–11]). The main feature of such scale-by-scale budget analysis is that the turbulent diffusion term is split into the spatial diffusion at each scale and the interscale transport at each spatial location, which allows us to

separately investigate the spatial and interscale transfer effects by the nonlinear scale interaction of turbulence.

Such scale-by-scale budget analysis of the turbulent energy transport has been used to study the complex energy transport in wall turbulence, and the behaviour of the interscale energy transport term was focused on in relation to the dynamics of coherent structures in the inner and outer layers. Particularly, in the spectral analysis of the energy transport, the analysis is possible based on either the streamwise and spanwise Fourier modes, and the interscale energy transport observed through the Fourier modes in different directions may represent different physical phenomena. It was suggested in Ref. [4] that the interscale energy transfers in the streamwise length scales likely represent the energy transfer associated with the self-sustaining cycles of each coherent structure in the inner and outer layer. On the other hand, the interscale energy transfers observed through the spanwise Fourier modes may represent the interactions between the inner and outer coherent structures. Many of the earlier studies on the scale-by-scale budget analysis were based on spanwise length scales, as the inner and outer structures have clearly different spanwise length scales [12]. It has been shown that the interscale energy transport terms exhibit both forward (from larger to smaller scales) and backward (from smaller to larger scales) energy transfers in the near-wall region [1,3,6,11,13,14], unlike in homogeneous isotropic turbulence, where the energy transfer is basically from larger to smaller scales. In particular, among these earlier studies, Kawata and Alfredsson [1] experimentally investigated a turbulent plane Couette flow and showed that the Reynolds shear stress is transferred from relatively small scales near the wall to large scales away from the wall. This observed transport of the Reynolds shear stress can be interpreted as the bottom-up influence from the inner to outer structure, which is in contrast to the general picture of turbulence that the energy is basically transferred from larger to smaller scales. Although the physical phenomenon represented by the inverse interscale transfer of the Reynolds shear stress has not been fully elucidated yet, some recent studies have suggested that the interscale energy transfer in the spanwise length scales is related to the interaction between the inner and outer structures [3,11,15].

The scale-by-scale analysis of the passive-scalar fluxes can also be performed in the almost same manner as the analysis of the Reynolds stress transport as their transport equations are similar. Such scale-by-scale analysis of passive-scalar transfer allows us to investigate the interscale and spatial transport of the passive scalar caused by nonlinear interactions between different scales in the velocity fields. However, despite numerous studies reported on the wall turbulence with a passive scalar field (e.g., Refs. [15–24]) in the last few decades, the scale-by-scale transport of the passive scalar in wall turbulence has not been explored yet.

In the present study, we extend the spanwise spectral analysis on the Reynolds stress transport in Ref. [1] to the turbulent heat flux transport. The transport equation budgets of the temperature-related spectra are investigated based on the direct numerical simulation (DNS) data of wall turbulence with a passive-scalar heat transfer, particularly focusing on if the transport from smaller scales near the wall to larger scales away from the wall is also investigated for turbulent heat fluxes similarly to the Reynolds stress transport. Turbulent plane Couette flow is chosen as the test case, because very-large-scale structures filling up the entire channel appear at relatively low Reynolds numbers [25–31], and therefore, scale separation between the inner and outer structures is relatively clearer than in other canonical wall-bounded flow configurations at the same Reynolds number. The constant-temperature-difference condition is adopted as the thermal boundary condition on the walls so that the mean velocity and temperature profiles are similar to each other. Then, fluctuating velocity and temperature fields are compared by focusing on the similarity/difference in the interscale and spatial energy transport caused by scale interactions. The analysis is based on the DNS data provided in our previous work [32], where the streamwise Fourier mode analysis was performed, and thereby, the interscale energy transfers associated with the self-sustaining cycle of coherent structures were compared

for the velocity and temperature fields. In this study, on the other hand, the spanwise spectral analysis is performed on the transport of the turbulent heat flux, and the interscale transfer of turbulent heat fluxes in spanwise length scales is investigated in relation to the interactions between the coherent structures in the inner and outer layers.

The layout of this paper is as follows: In Section 2, the numerical setup for the DNS is briefly described, and the spectral transport equations of the temperature-related statistics are introduced. In Section 3, the results of the spectral budget analysis are presented. First, the distributions of the turbulent energy and temperature-related spectra are shown, followed by the corresponding interscale and spatial fluxes. Then, the budget balance of the transport equations of the temperature-related spectra are investigated in comparison with those of the corresponding Reynolds stress component. Finally, in Section 4, a discussion and concluding remarks are given.

2. DNS Dataset and Spectral Budget Analysis

2.1. DNS Dataset of a Turbulent Plane Couette Flow with Temperature Transport

In the present study, the budget analysis of the spectral transport equations is performed with a DNS dataset of a turbulent plane Couette flow with passive-scalar temperature transport obtained in our previous work [32]. Here, we briefly summarise the computational conditions. The geometrical configuration of the plane Couette flow is such that a shear flow is driven by the stationary bottom wall and the top wall translating with a constant speed U_w, which are separated by a distance h. The x-, y-, and z-axes are taken in the streamwise, wall-normal, and spanwise directions, and the origin of the coordinates is placed on the stationary bottom wall; the bottom and top walls are located at $y = 0$ and $y = h$, respectively. The temperatures of the walls are uniform and constant in time, and the temperature difference is $\Delta T = T_t - T_b$ (T_t and T_b are the temperature of the top and the bottom walls, respectively).

The governing equations of fluid flow are the continuity and Navier-Stokes equations for incompressible flow that are non-dimensionalised by h and U_w, and the convection-diffusion equation of passive-scalar temperature non-dimensionalised by ΔT, h, and U_w is solved for the fluctuating temperature field. A non-slip boundary condition is applied to the fluid velocity on the wall, and as described above, the temperature on the walls is uniform and constant in time with the temperature difference ΔT. It should be noted here that both the velocity and temperature fields are driven by a uniform and constant velocity or temperature difference between the top and bottom walls, and therefore, the boundary conditions on the walls for the velocity and temperature fields are similar when scaled by the velocity difference U_w and the temperature difference ΔT, respectively. For the streamwise and spanwise directions, periodic boundary conditions are applied. The Reynolds number $Re_w = U_w h / \nu$ and Prandtl number $Pr = \alpha / \nu$ are $Re_w = 8600$ and $Pr = 0.71$, where ν and α are the kinematic viscosity and the thermal diffusivity of the fluid, respectively, and other details of the DNS, such as the domain size and spatial resolution, are listed in Table 1.

Table 1. Computational conditions: streamwise and spanwise domain lengths, number of grid points, spatial resolutions, and the friction Reynolds number $Re_\tau = u_\tau \delta / \nu$ ($u_\tau = \sqrt{\tau_w / \rho}$, $\delta = h/2$). The Reynolds number and Prandtl number are $Re_w = 8600$ and $Pr = 0.71$, respectively.

(L_x, Lz)	(N_x, N_y, Nz)	$(\Delta x^+, \Delta z^+)$	$(\Delta y^+_{max}, \Delta y^+_{min})$	Re_τ
$(24\,h, 12.8\,h)$	$(512, 96, 512)$	$(11.8, 6.31)$	$(6.16, 0.268)$	126.1

We denote the velocity components in the x-, y-, and z-directions as $U + u$, v, w, respectively. Here, U is the mean streamwise velocity, and the lower-case letter represents the fluctuation around the mean value of each velocity component (note here that the mean wall-normal and spanwise velocities are zero). The temperature is defined as the temperature difference between the fluid and the bottom wall and denoted as $\Theta + \theta$:

here, Θ and θ are the mean temperature and the temperature fluctuation, respectively, and $\Theta = 0$ and ΔT at the bottom and top walls, respectively. In the following, $\langle \rangle$ represents averaged quantities obtained by averaging in x- and z-directions and in time. They are also averaged between the lower and upper half of the channel because of the symmetric flow configuration.

Figures 1 and 2 show the profiles of the mean velocity and temperature and those of the second-order statistics, such as velocity and temperature variances and their cross correlations. Here, T_τ used in Figure 1b is the friction temperature defined as $T_\tau = Q_w/\rho c_p u_\tau$, where Q_w and c_p are the mean heat flux on the wall and the specific heat at constant pressure, respectively, and u_τ is the friction velocity defined as $u_\tau = \sqrt{\tau_w/\rho}$ (τ_w and ρ are the wall shear stress and the fluid density). As shown in Figure 1a, the profile of the mean temperature Θ is anti-symmetric, similarly to the mean velocity profile due to the similar boundary conditions for the velocity and temperature fields, and it is also seen in Figure 1b that the mean temperature gradient $\mathrm{d}\Theta/\mathrm{d}y$ in the vicinity of the wall is markedly smaller than the mean streamwise velocity gradient $\mathrm{d}U/\mathrm{d}y$. This difference can be attributed to the fact that $Pr = 0.71 < 1$, which makes the effect of molecular diffusion more significant in the temperature field than in the velocity field.
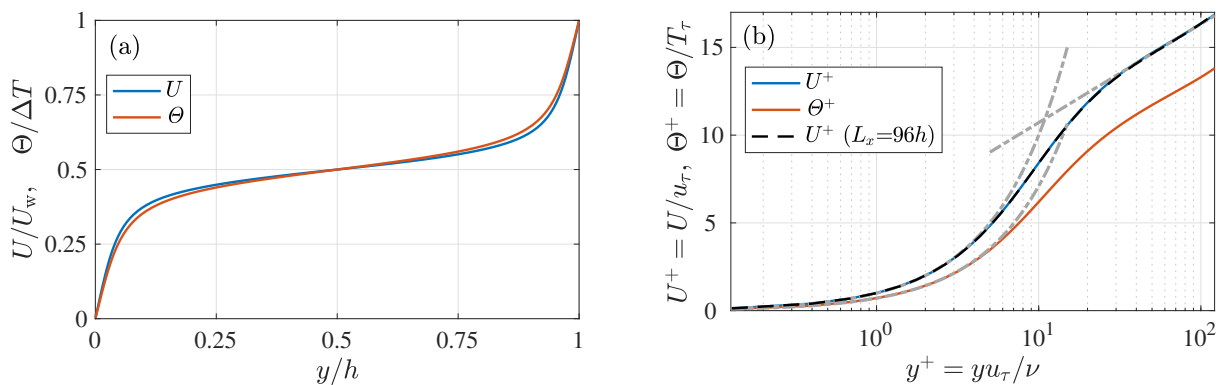

Figure 1. Profiles of mean streamwise velocity U and the mean temperature Θ in (**a**) outer and (**b**) inner scaling. In panel (**b**), the grey chained lines indicate $U^+ = y^+$ and $U^+ = 2.44 \ln y^+ + 5.1$ for the mean velocity profile and $\Theta^+ = Pr y^+$ for the mean temperature profile, and the black dashed line presents the profile of mean velocity U^+ obtained with an extremely large computational domain $(L_x, L_z) = (96.0\,h, 12.8\,h)$ in Ref. [4].
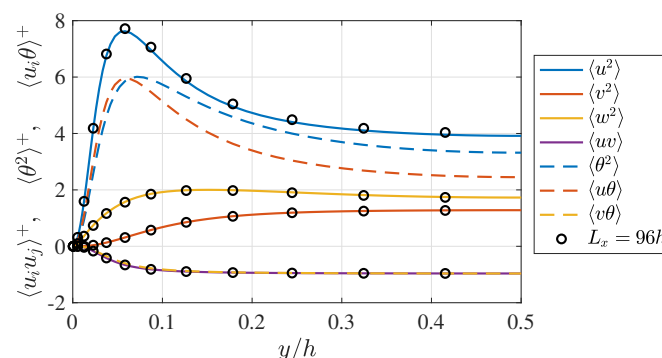

Figure 2. Profiles of (solid lines) the Reynolds stresses $\langle u_i u_j \rangle$ and (dashed lines) the temperature-related turbulent statistics $\langle \theta^2 \rangle$ and $\langle u_i \theta \rangle$. The values are scaled based on the inner units, u_τ and/or T_τ, and only $0 \ll y \ll 0.5$ is shown. The black circles present profiles of the Reynolds stresses obtained with an extremely large computational domain $(L_x, L_z) = (96\,h, 12.8\,h)$ in Ref. [4].

Figure 2 presents the profiles of the Reynolds stresses $\langle u^2 \rangle$, $\langle v^2 \rangle$, $\langle w^2 \rangle$, and $\langle uv \rangle$, and the temperature-related statistics: the temperature fluctuation $\langle \theta^2 \rangle$ and the velocity-temperature correlations $\langle u\theta \rangle$ and $\langle v\theta \rangle$. As shown here, the temperature fluctuation $\langle \theta^2 \rangle$

and the streamwise-velocity-temperature correlation $\langle u\theta \rangle$ have similar profiles to the streamwise velocity fluctuation $\langle u^2 \rangle$, which indicates a certain similarity between the fluctuations of the streamwise velocity u and of the temperature θ. This is attributable to the fact that the profiles of the mean streamwise velocity U and mean temperature Θ are similar. It is also shown here that the profiles of the Reynolds shear stress $\langle uv \rangle$ and turbulent heat flux $\langle v\theta \rangle$ are almost on top of each other, which indicates a strong similarity between the turbulent momentum and the heat transfers. It should be noted that the cross correlations related to the spanwise velocity w, such as $\langle uw \rangle$ and $\langle w\theta \rangle$, are negligibly small in magnitude compared to $-\langle uv \rangle$ and $-\langle v\theta \rangle$, although the spanwise velocity variance $\langle w^2 \rangle$ is certainly larger than that of the wall-normal velocity $\langle v^2 \rangle$, and these cross correlations related to w are, therefore, not investigated in the present study.

In the DNS of turbulent plane Couette flow, one needs to use a considerably large computational domain to exclude the dependency of the obtained DNS results on the computational domain size due to the very-large-scale structure [25]. The effect of the domain size was carefully addressed in our previous work [4], and it was confirmed that the domain size used for obtaining the present DNS dataset, $(L_x, L_z) = (24.0\ h, 12.8\ h)$, was large enough to exclude the domain-size effect, as demonstrated in Figures 1 and 2 by the good agreement between the present computational results and those obtained with a much larger computational domain in Ref. [4].

2.2. Spectral Analysis of the Reynolds-Stress Transport and Turbulent Heat Transfers

In the present study, the spectral transports of the temperature fluctuation $\langle \theta^2 \rangle$ and the turbulent heat fluxes $\langle u_i\theta \rangle$ are analysed based on spanwise Fourier mode analysis. The transport equations of the temperature-related spectra are derived similarly to those for the Reynolds stress spectra. Here, the derivation of the transport equations of the Reynolds stress spectra is briefly reviewed, and the spectral transport equations for the temperature-related statistics are introduced by similar means.

2.2.1. Transport of Reynolds Stresses

The transport of the Reynolds stresses $\langle u_i u_j \rangle$ is expressed as

$$\left(\frac{\partial}{\partial t} + U_k \frac{\partial}{\partial x_k} \right) \langle u_i u_j \rangle = P_{ij} - \varepsilon_{ij} + \Phi_{ij} + D_{ij}^v + D_{ij}^t, \tag{1}$$

where the terms on the right-hand side are the production (P_{ij}), viscous dissipation (ε_{ij}), pressure-gradient work (Φ_{ij}), viscous diffusion (D_{ij}^v), and turbulent diffusion (D_{ij}^t) terms, which are defined as

$$P_{ij} = -\langle u_i u_k \rangle \frac{\partial U_j}{\partial x_k} - \langle u_j u_k \rangle \frac{\partial U_i}{\partial x_k}, \quad \varepsilon_{ij} = 2\nu \left\langle \frac{\partial u_i}{\partial x_k} \frac{\partial u_j}{\partial x_k} \right\rangle, \tag{2}$$

$$\Phi_{ij} = -\left\langle \frac{\partial p}{\partial x_i} u_j \right\rangle - \left\langle \frac{\partial p}{\partial x_j} u_i \right\rangle, \quad D_{ij}^v = \nu \frac{\partial^2 \langle u_i u_j \rangle}{\partial x_k^2}, \quad D_{ij}^t = -\frac{\partial \langle u_i u_j u_k \rangle}{\partial x_k}. \tag{3}$$

The pressure term Φ_{ij} may be decomposed into the pressure-strain correlation Π_{ij} and the pressure diffusion D_{ij}^p:

$$\Phi_{ij} = \Pi_{ij} + D_{ij}^p, \text{ where } \Pi_{ij} = \left\langle p \left(\frac{\partial u_i}{\partial x_j} + \frac{\partial u_j}{\partial x_i} \right) \right\rangle \text{ and } D_{ij}^p = -\frac{\partial}{\partial x_k} \left(\langle u_i p \rangle \delta_{jk} + \langle u_j p \rangle \delta_{ik} \right). \tag{4}$$

δ_{ij} is the Kronecker's delta.

Now, we introduce a decomposition of the fluctuating components into their large- and small-scale parts as

$$u_i = u_i^L + u_i^S, \quad \theta = \theta^L + \theta^S, \tag{5}$$

based on the spanwise Fourier-mode decomposition, where u_i^L and θ^L consist of the spanwise Fourier modes at smaller wavenumbers than a cutoff wavenumber $k_{z,c}$, while u_i^S and θ^S comprise the rest: $u_i^S = u_i - u_i^L$, $\theta^S = \theta - \theta^L$. With such a decomposition, there is no overlapping wavenumber range between the large- and small-scale quantities. Hence, the cross correlation between them is zero for any combination of quantities:

$$\left\langle u_i^L u_j^S \right\rangle = \left\langle u_j^L u_i^S \right\rangle = 0, \quad \left\langle \theta^L \theta^S \right\rangle = \left\langle u_i^L \theta^S \right\rangle = \left\langle u_i^S \theta^L \right\rangle = 0. \tag{6}$$

Equation (6) is mathematically satisfied if the decomposition (5) is based on an orthogonal mode decomposition and the large- and small-scale quantities do not have any mode in common, which is the case in the present study. Similar decomposition is also possible based on other orthogonal mode decomposition methods, for example, the proper orthogonal mode decomposition.

As the cross correlations between the large- and small-scale quantities are zero as described above, the Reynolds stresses $\langle u_i u_j \rangle$ are decomposed simply into their large- and small-scale parts as

$$\langle u_i u_j \rangle = \left\langle u_i^L u_j^L \right\rangle + \left\langle u_i^S u_j^S \right\rangle, \tag{7}$$

and by a similar manner, to derive the "full" Reynolds stress Equation (1), one obtains the transport equations of the large- and small-scale parts of the Reynolds stresses (the details of the derivation are found in Refs. [4,33]) as

$$\left(\frac{\partial}{\partial t} + U_k \frac{\partial}{\partial x_k} \right) \left\langle u_i^L u_j^L \right\rangle = P_{ij}^L - \varepsilon_{ij}^L + \Phi_{ij}^L + D_{ij}^{\nu,L} + D_{ij}^{t,L} - Tr_{ij}^z, \tag{8}$$

$$\left(\frac{\partial}{\partial t} + U_k \frac{\partial}{\partial x_k} \right) \left\langle u_i^S u_j^S \right\rangle = P_{ij}^S - \varepsilon_{ij}^S + \Phi_{ij}^S + D_{ij}^{\nu,S} + D_{ij}^{t,S} + Tr_{ij}^z. \tag{9}$$

The terms on the right-hand sides of Equations (8) and (9) are the large- and small-scale parts of their counterpart in Equation (1), except for Tr_{ij}. In particular, the first four terms on the right-hand side of each equation (i.e., the production, viscous dissipation, pressure-gradient work, and viscous diffusion) are simply decomposed into their large- and small-scale parts, similarly to the Reynolds stress decomposition in Equation (7): these terms in Equation (8) are defined as those in Equation (1)–(3) with u_i and u_j replaced by u_i^L and u_j^L (the corresponding terms in Equation (9) are similarly defined by u_i^S and u_j^S).

On the other hand, the turbulent diffusion is decomposed as

$$D^{t,L} = -\frac{\partial \langle u_i u_j u_k \rangle^L}{\partial x_k}, \quad D^{t,S} = -\frac{\partial \langle u_i u_j u_k \rangle^S}{\partial x_k}, \tag{10}$$

where $\langle u_i u_j u_k \rangle^L$ and $\langle u_i u_j u_k \rangle^S$ are, respectively, the large- and small-scale part of the triple velocity correlation $\langle u_i u_j u_k \rangle$ defined as

$$\langle u_i u_j u_k \rangle^L = \left\langle u_i^L u_j^L u_k^L \right\rangle + \left\langle u_i^L u_j^L u_k^S \right\rangle + \left\langle u_i^S u_j^L u_k^S \right\rangle + \left\langle u_i^L u_j^S u_k^S \right\rangle, \tag{11}$$

$$\langle u_i u_j u_k \rangle^S = \left\langle u_i^S u_j^S u_k^S \right\rangle + \left\langle u_i^S u_j^S u_k^L \right\rangle + \left\langle u_i^L u_j^S u_k^L \right\rangle + \left\langle u_i^S u_j^L u_k^L \right\rangle. \tag{12}$$

Note here that the triple correlations in Equations (11) and (12), including both the large- and small-scale parts, such as $\left\langle u_i^L u_j^L u_k^S \right\rangle$ and $\left\langle u_i^S u_j^L u_k^S \right\rangle$, are not zero unlike the second-

order cross correlations $\left\langle u_i^L u_j^S \right\rangle$ and $\left\langle u_i^S u_j^L \right\rangle$. The last term in Equations (8) and (9), Tr_{ij}^z, is defined as

$$Tr_{ij}^z = -\left\langle u_i^S u_k^S \frac{\partial u_j^L}{\partial x_k} \right\rangle - \left\langle u_j^S u_k^S \frac{\partial u_i^L}{\partial x_k} \right\rangle + \left\langle u_i^L u_k^L \frac{\partial u_j^S}{\partial x_k} \right\rangle + \left\langle u_j^L u_k^L \frac{\partial u_i^S}{\partial x_k} \right\rangle. \tag{13}$$

It is observed from Equations (8) and (9) that this term appears in the transport equations of both $\left\langle u_i^L u_j^L \right\rangle$ and $\left\langle u_i^S u_j^S \right\rangle$ with different signs, which means that Tr_{ij}^z represents the energy flux between the large- and small-scale velocity fields across the cutoff wavenumber $k_{z,c}$.

It is worth pointing out here that only the turbulent diffusion terms ($D_{ij}^{t,L}$ and $D_{ij}^{t,S}$) and the interscale energy flux term (Tr_{ij}^z) include both the large- and small-scale parts of the fluctuating velocities, whereas the other terms in the transport equations consist of either the large- or small-scale part only. This is because the turbulent transport and the interscale energy flux terms are the third-order moments of the fluctuating velocities (and the velocity gradients), while the other terms are second-order moments. These terms including both the large- and small-scale parts of the fluctuating velocity can be interpreted as the energy transport effects by interactions between different scales: the turbulent transport ($D_{ij}^{t,L}$ and $D_{ij}^{t,S}$) indicates the energy transport in physical space caused by scale interactions, while the interscale energy flux (Tr_{ij}^z) is the energy transport between different scales.

As the large-scale part of the Reynolds stresses $\left\langle u_i^L u_j^L \right\rangle$ and the spanwise one-dimensional spectra of the Reynolds stresses are related as

$$E_{ij}^z = \frac{\partial \left\langle u_i^L u_j^L \right\rangle}{\partial k_{z,c}} \left(= -\frac{\partial \left\langle u_i^S u_j^S \right\rangle}{\partial k_{z,c}} \right), \tag{14}$$

the transport equations of the Reynolds-stress spectra can be derived by differentiating both sides of Equation (8) with respect to $k_{z,c}$ as

$$\left(\frac{\partial}{\partial t} + U_k \frac{\partial}{\partial x_k} \right) E_{ij}^z = pr_{ij}^z - \xi_{ij}^z + \phi_{ij}^z + d_{ij}^{v,z} + d_{ij}^{t,z} + tr_{ij}^z, \tag{15}$$

where the terms on the right-hand side are the $k_{z,c}$-derivatives of the counter parts in Equation (8). The first five terms represent the spectra of the corresponding terms of Equation (1): the spectra of the production (pr_{ij}^z), viscous dissipation (ξ_{ij}^z), pressure term (ϕ_{ij}^z), viscous diffusion ($d_{ij}^{v,z}$) and turbulent diffusion ($d_{ij}^{t,z}$) terms. The interscale transport term tr_{ij}^z represents the energy gain/loss by the interscale flux Tr_{ij} at each wavenumebr k_z. According to Equation (4), the pressure-gradient-work spectrum ϕ_{ij} can also be decomposed into the spectra of the pressure-strain energy redistribution term Π_{ij} and the pressure diffusion term D_{ij}^p as

$$\phi_{ij}^z = \pi_{ij}^z + d_{ij}^{p,z}. \tag{16}$$

The turbulent spatial transport $d_{ij}^{t,z}$ and the interscale transport tr_{ij}^z, which are of particular interest in the present study, are defined as

$$d_{ij}^{z,t} = -\frac{\partial E_{ijk}^z}{\partial x_k}, \qquad tr_{ij}^z = -\frac{\partial Tr_{ij}^z}{\partial k_{z,c}}. \tag{17}$$

Here, E_{ijk}^z is the spectra of triple velocity correlations $\langle u_i u_j u_k \rangle$ defined as

$$E_{ijk}^z = \frac{\partial \langle u_i u_j u_k \rangle^L}{\partial k_{z,c}} = -\frac{\partial \langle u_i u_j u_k \rangle^S}{\partial k_{z,c}}. \tag{18}$$

As the physical meaning of $\langle u_i u_j u_k \rangle$ is the spatial transport flux of the Reynolds stress $\langle u_i u_j \rangle$ in the x_k-direction caused by the velocity fluctuation u_k, their spectra E_{ijk}^z represent the spatial flux of the Reynolds stresses $\langle u_i u_j \rangle$ in the x_k-direction at each spanwise wavenumber.

In order to evaluate the terms on the right-hand side of Equation (10), the procedure to decompose the velocity and temperature fluctuations as in Equations (5) by applying a spatial filter is repeated for all possible values of $k_{z,c}$, i.e., $k_{z,c} = 2\pi/L_x, 4\pi/L_x, 6\pi/L_x, \cdots$, and all terms on the right-hand side of Equation (8) are evaluated for each value of the cutoff wavenumber $k_{z,c}$. Then, the derivatives with respect to $k_{z,c}$ are evaluated for all terms at each $k_{z,c}$, and thus the terms on the right-hand side of Equation (10) are obtained as functions of the wall-normal position y and the spanwise wavenumber k_z (or the spanwise wavelength $\lambda_z = 2\pi/k_z$).

2.2.2. Transport of Temperature Fluctuation and Velocity-Temperature Correlations

Now, we derive the spectral transport equations of the temperature-related turbulence statistics. The transport equation of the temperature fluctuation $\langle \theta^2 \rangle$ is written similarly to the Reynolds stress Equation (1) as

$$\left(\frac{\partial}{\partial t} + U_k \frac{\partial}{\partial x_k} \right) \langle \theta^2 \rangle = P_{\theta\theta} - \varepsilon_{\theta\theta} + D_{\theta\theta}^v + D_{\theta\theta}^t, \tag{19}$$

with the production ($P_{\theta\theta}$), viscous dissipation ($\varepsilon_{\theta\theta}$), viscous diffusion ($D_{\theta\theta}^v$), and turbulent transport ($D_{\theta\theta}^t$) terms defined as

$$P_{\theta\theta} = -2\langle \theta u_k \rangle \frac{\partial \Theta}{\partial x_k}, \quad \varepsilon_{\theta\theta} = 2\alpha \left\langle \frac{\partial \theta}{\partial x_k} \frac{\partial \theta}{\partial x_k} \right\rangle, \quad D_{ij}^v = \alpha \frac{\partial^2 \langle \theta^2 \rangle}{\partial x_k^2}, \quad D_{\theta\theta}^t = -\frac{\partial \langle \theta^2 u_k \rangle}{\partial x_k}. \tag{20}$$

The transport equation of the turbulent heat fluxes $\langle u_i \theta \rangle$ is also similarly obtained as

$$\left(\frac{\partial}{\partial t} + U_k \frac{\partial}{\partial x_k} \right) \langle u_i \theta \rangle = P_{i\theta} - \varepsilon_{i\theta} + \Phi_{i\theta} + D_{i\theta}^v + D_{i\theta}^t, \tag{21}$$

with the production ($P_{i\theta}$), viscous dissipation ($\varepsilon_{i\theta}$), pressure-gradient-temperature correlations ($\Phi_{i\theta}$), viscous diffusion ($D_{i\theta}^v$), and turbulent diffusion ($D_{i\theta}^t$) terms defined as

$$P_{i\theta} = -\langle u_k \theta \rangle \frac{\partial U_i}{\partial x_k} - \langle u_i u_k \rangle \frac{\partial \Theta}{\partial x_k}, \quad \varepsilon_{i\theta} = (\nu + \alpha) \left\langle \frac{\partial u_i}{\partial x_k} \frac{\partial \theta}{\partial x_k} \right\rangle, \quad \Phi_{i\theta} = -\left\langle \frac{\partial p}{\partial x_i} \theta \right\rangle, \tag{22}$$

$$D_{i\theta}^v = \frac{\partial}{\partial x_k} \left(\nu \left\langle \frac{\partial u_i}{\partial x_k} \theta \right\rangle + \alpha \left\langle \frac{\partial \theta}{\partial x_k} u_i \right\rangle \right), \quad D_{i\theta}^t = -\frac{\partial \langle u_i \theta u_k \rangle}{\partial x_k}. \tag{23}$$

Based on the decomposition given by Equation (5), the temperature variance and the turbulent heat fluxes are also split into their large- and small-scale parts, similarly to the Reynolds stress decomposition (7), as

$$\langle \theta^2 \rangle = \left\langle \theta^L \theta^L \right\rangle + \left\langle \theta^S \theta^S \right\rangle, \quad \langle u_i \theta \rangle = \left\langle u_i^L \theta^L \right\rangle + \left\langle u_i^S \theta^S \right\rangle. \tag{24}$$

Therefore, the transport equations of their large- and small-scale parts can be derived similarly to Equations (8) and (9). Then, these large- and small-scale parts of the temperature-related statistics are related to their spectra, similarly to Equation (14), as

$$E_{\theta\theta}^z = \frac{\partial\langle\theta^L\theta^L\rangle}{\partial k_{z,c}}, \quad E_{i\theta}^z = \frac{\partial\langle u_i^L\theta^L\rangle}{\partial k_{z,c}}, \tag{25}$$

and the transport equations of these temperature-related spectra can also be obtained by differentiating the equations of $\langle\theta^L\theta^L\rangle$ and $\langle u_i^L\theta^L\rangle$. With such procedures, one obtains the temperature-variance spectrum equation as

$$\left(\frac{\partial}{\partial t} + U_k\frac{\partial}{\partial x_k}\right)E_{\theta\theta}^z = pr_{\theta\theta}^z - \xi_{\theta\theta}^z + d_{\theta\theta}^{\nu,z} + d_{\theta\theta}^{t,z} + tr_{\theta\theta}^z, \tag{26}$$

with the terms on the right-hand side representing the spectra of the counterparts in Equation (19). The interscale and the turbulent spatial transport terms are defined as

$$tr_{\theta\theta}^z = -\frac{\partial Tr_{\theta\theta}^z}{\partial k_{z,c}}, \qquad d_{\theta\theta}^{t,z} = -\frac{\partial E_{\theta\theta k}^z}{\partial x_k}, \tag{27}$$

where $Tr_{\theta\theta}^z$ and $E_{\theta\theta k}^z$ are the interscale and spectral spatial fluxes of the temperature fluctuation defined as

$$Tr_{\theta\theta}^z = -2\left\langle\theta^S u_k^S\frac{\partial\theta^L}{\partial x_k}\right\rangle - 2\left\langle\theta^L u_k^L\frac{\partial\theta^S}{\partial x_k}\right\rangle, \tag{28}$$

$$E_{\theta\theta k}^z = \frac{\partial\langle\theta^2 u_k\rangle^L}{\partial k_{z,c}} = -\frac{\partial\langle\theta^2 u_k\rangle^S}{\partial k_{z,c}}, \tag{29}$$

with $\langle\theta^2 u_k\rangle^L$ and $\langle\theta^2 u_k\rangle^S$ being the large- and small-scale part of the spatial flux of the temperature fluctuation $\langle\theta^2 u_k\rangle$:

$$\langle\theta^2 u_k\rangle^L = \langle\theta^L\theta^L u_k^L\rangle + \langle\theta^L\theta^L u_k^S\rangle + 2\langle\theta^L\theta^S u_k^S\rangle, \tag{30}$$

$$\langle\theta^2 u_k\rangle^S = \langle\theta^S\theta^S u_k^S\rangle + \langle\theta^S\theta^S u_k^L\rangle + 2\langle\theta^L\theta^S u_k^L\rangle. \tag{31}$$

Similarly, the transport equation of the turbulent heat flux spectrum $E_{i\theta}^z$ is obtained as

$$\left(\frac{\partial}{\partial t} + U_k\frac{\partial}{\partial x_k}\right)E_{i\theta}^z = pr_{i\theta}^z - \xi_{i\theta}^z + \phi_{i\theta}^z + d_{i\theta}^{\nu,z} + d_{i\theta}^{t,z} + tr_{i\theta}^z, \tag{32}$$

and the terms on the right-hand side are, again, the spectra of their counterparts in Equation (21). The interscale and the turbulent spatial transport terms are defined in the same manner as in other spectral transport equations:

$$tr_{i\theta}^z = -\frac{\partial Tr_{i\theta}^z}{\partial k_{z,c}}, \qquad d_{i\theta}^{t,z} = -\frac{\partial E_{i\theta k}^z}{\partial x_k}, \tag{33}$$

where the interscale flux $Tr_{i\theta}^z$ and spectral spatial flux $E_{i\theta k}^z$ are, respectively, defined as

$$Tr_{i\theta}^z = -\left\langle\theta^S u_k^S\frac{\partial u_i^L}{\partial x_k}\right\rangle - \left\langle u_i^S u_k^S\frac{\partial\theta^L}{\partial x_k}\right\rangle + \left\langle\theta^L u_k^L\frac{\partial u_i^S}{\partial x_k}\right\rangle + \left\langle u_i^L u_k^L\frac{\partial\theta^S}{\partial x_k}\right\rangle, \tag{34}$$

$$E_{i\theta k}^z = \frac{\partial\langle u_i\theta u_k\rangle^L}{\partial k_{z,c}} = -\frac{\partial\langle u_i\theta u_k\rangle^S}{\partial k_{z,c}}. \tag{35}$$

Here, $\langle u_i \theta u_k \rangle^L$ and $\langle u_i \theta u_k \rangle^S$ are the large- and small-scale parts of $\langle u_i \theta u_k \rangle$ defined as

$$\langle u_i \theta u_k \rangle^L = \left\langle u_i^L \theta^L u_k^L \right\rangle + \left\langle u_i^L \theta^L u_k^S \right\rangle + \left\langle u_i^L \theta^S u_k^S \right\rangle + \left\langle u_i^S \theta^L u_k^S \right\rangle, \tag{36}$$

$$\langle u_i \theta u_k \rangle^S = \left\langle u_i^S \theta^S u_k^S \right\rangle + \left\langle u_i^S \theta^S u_k^L \right\rangle + \left\langle u_i^S \theta^L u_k^L \right\rangle + \left\langle u_i^L \theta^S u_k^L \right\rangle. \tag{37}$$

The terms on the right-hand side of Equations (17) and (19) are obtained in a similar manner as those of Equation (10): Repeating the decomposition (5) for all possible values of the cutoff wavenumber $k_{z,c}$, evaluating all terms in the transport equations of $\left\langle \theta^L \theta^L \right\rangle$ and $\left\langle u_i^L \theta^L \right\rangle$ at each $k_{z,c}$, and evaluating the $k_{c,z}$-derivatives of all terms at each $k_{z,c}$.

3. Results

3.1. Spectra of Temperature-Related Statistics and Their Interscale and Spatial Transports

Figure 3 presents the distributions of the spanwise one-dimensional spectra of the streamwise turbulent energy E_{uu}^z, temperature fluctuation $E_{\theta\theta}^z$, and temperature-velocity correlation $E_{u\theta}^z$ in the premultiplied form. The distribution of the streamwise turbulent energy spectrum E_{uu}^z in the panel (a) shows two significant energy concentrations, one of which is the energy peak located in a relatively small wavelength range near the wall around $(y^+, \lambda_z^+) \approx (12, 100)$ and the other is the broad energy band at a large wavelength around $\lambda_z/h \approx 2.5$ covering most of the channel. Here, λ_z^+ is the spanwise wavenumber scaled by viscous length scale ν/u_τ. These energy peaks clearly correspond to the small-scale coherent structures near the wall and the very-large-scale structure of plane Couette turbulence, respectively. As shown in this figure, the energy peaks corresponding to these coherent structures at different scales are observed to be clearly separated from each other despite the relatively small Reynolds number $Re_\tau = 126$, which is a unique feature of plane Couette turbulence [26–28].
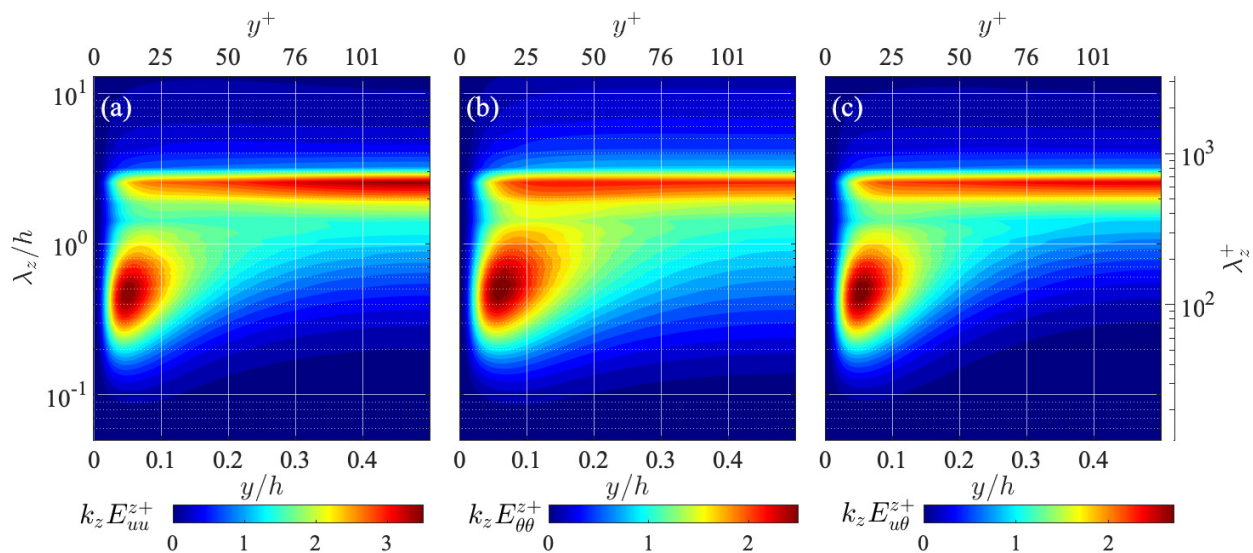

Figure 3. Space-wavelength ($y - \lambda_z$) diagrams of spanwise one-dimensional premultiplied spectra of (**a**) streamwise turbulent energy $k_z E_{uu}^z$, (**b**) temperature fluctuation $k_z E_{\theta\theta}^z$, and (**c**) velocity-temperature correlation $k_z E_{u\theta}^z$. The values are scaled by u_τ^2, T_τ^2, and $u_\tau T_\tau$, respectively.

The temperature-fluctuation spectrum $E_{\theta\theta}^z$ presents a similar distribution to the streamwise turbulent energy E_{uu}^z, as shown in Figure 3b, in which the energy peaks corresponding to the near-wall and very-large-scale structures are indicated at almost the same position in the y-λ_z diagram. The location of the near-wall peak is, however, at a slightly larger wavelength and further from the wall than the corresponding peak in the E_{uu}^z distribution, $(y^+, \lambda_z^+) \approx (16, 134)$, which can be attributed to the more significant effect of molecular diffusion in the temperature field as $Pr < 1$. The distribution of the temperature-velocity

cospectrum $E^z_{u\theta}$ also shows a similar distribution to E^z_{uu}, indicating similar behaviours of the fluctuating streamwise velocity and temperature.

Figure 4 compares the spanwise one-dimensional cospectra of the Reynolds shear stress E^z_{-uv} and the velocity-temperature correlation $E^z_{-v\theta}$. As the Reynolds shear stress $-\langle uv \rangle$ and the temperature-velocity correlation $-\langle v\theta \rangle$ represent the wall-normal transport of momentum and heat by turbulent fluid motions, respectively, their cospectra represent the turbulent momentum and heat transfers at each length scale. As shown in Figure 4a, the distribution of the Reynolds shear stress cospectrum E^z_{-uv} presents both the inner peak at small scales near the wall and the broad energy peak at large scales at the channel centre, similarly to the distribution of the streamwise turbulent energy spectrum E^z_{uu}. As shown in Figure 4b, the distribution of the turbulent heat transfer spectrum $E^z_{-v\theta}$ is qualitatively similar to that of the momentum transfer spectrum E^z_{-uv}, presenting both the inner and outer energy peaks corresponding to the coherent structures in the near-wall and channel-central regions of the channel, which indicates a certain scale-by-scale similarity between the momentum and heat transfers by turbulence.
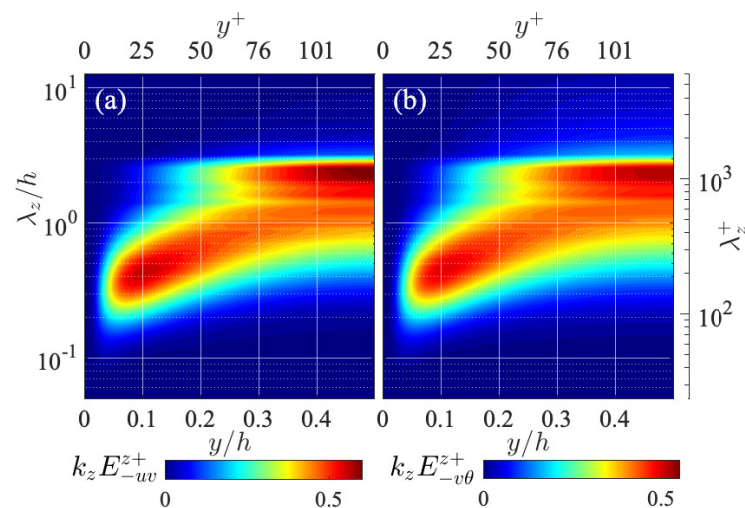

Figure 4. Spanwise one-dimensional spectra of (**a**) the Reynolds shear stress E^z_{-uv} and (**b**) turbulent heat transfer $E^z_{-v\theta}$, presented in the same manner as in Figure 3.

3.2. Interscale Fluxes of the Reynolds Stresses and Temperature-Related Statistics

Next, the interscale fluxes of the temperature-related spectra are investigated. Figure 5 presents the distributions of the spanwise interscale flux of the streamwise turbulent energy Tr^z_{uu}, temperature fluctuation $Tr^z_{\theta\theta}$, and temperature-velocity correlation $Tr^z_{u\theta}$. Here, as can be seen from Equations (8) and (9), the positive values indicate forward energy fluxes (i.e., from larger to smaller scales) in the spanwise length-scale direction, whereas the negative values represent the inverse (from smaller to larger scales) energy fluxes. As shown in Figure 5a, the turbulent energy flux Tr^z_{uu} indicates mainly forward interscale energy transfers from larger to smaller λ_z in the relatively small λ_z range throughout the channel, but it also presents backward energy fluxes from smaller to larger λ_z in a relatively large λ_z range in the near-wall region. It is interesting to note that such inverse interscale energy transfer is not observed in the streamwise length-scale direction [4,7], and the corresponding physical phenomenon has still not been elucidated.

As shown in Figure 5b, the spanwise interscale flux of the temperature fluctuation $Tr^z_{\theta\theta}$ presents a qualitatively similar distribution to the streamwise turbulent energy flux Tr^z_{uu}, presenting a region of backward interscale energy transfers at relatively large λ_z in the near-wall region and forward interscale energy fluxes at smaller λ_z throughout the channel. One can, however, also observe in the distribution of $Tr^z_{\theta\theta}$ that the region of backward energy flux somewhat shrinks, and instead, the magnitude of the forward energy flux around the channel centre is relatively stronger than Tr^z_{uu}.
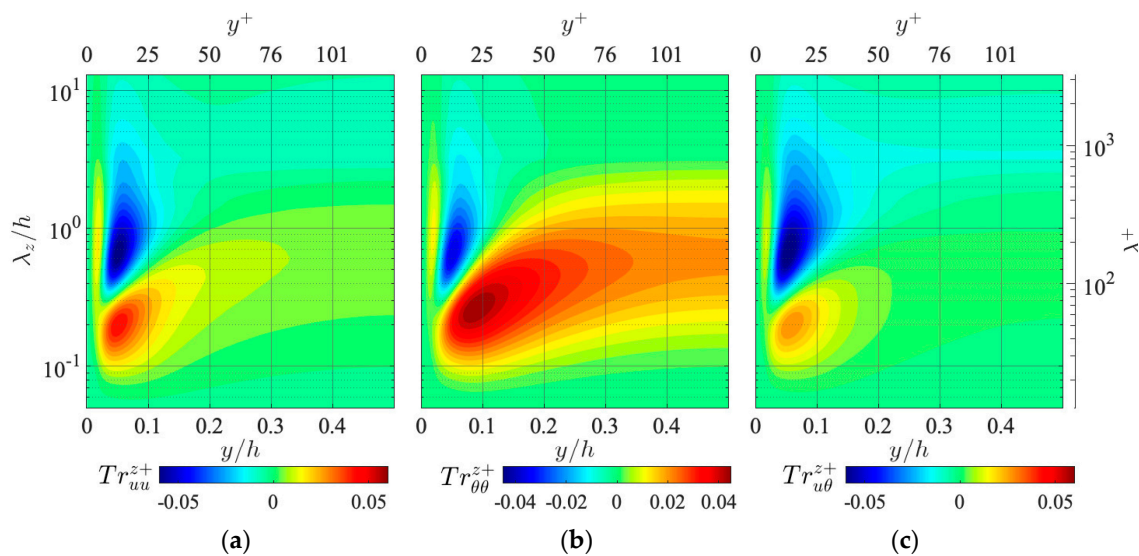
Figure 5. Space-wavelength $(y - \lambda_z)$ diagrams of spanwise interscale fluxes of (**a**) the turbulent kinetic energy Tr^z_{uu}, (**b**) temperature fluctuation $Tr^z_{\theta\theta}$, and (**c**) temperature-velocity correlation $Tr^z_{u\theta}$. The values are scaled by u^4_τ/ν, u^2_τ, T^2_τ/ν, and $u^3_\tau T_\tau/\nu$, respectively.

Figure 5c shows the distribution of the spanwise interscale flux of the velocity-temperature correlation $Tr^z_{u\theta}$. One can observe that $Tr^z_{u\theta}$ also has a qualitatively similar distribution to those of the turbulent energy flux Tr^z_{uu} and the temperature fluctuation flux $Tr^z_{\theta\theta}$, presenting both a backward and forward energy flux. Furthermore, as compared to the distributions of Tr^z_{uu} and $Tr^z_{\theta\theta}$, the region of backward energy flux is relatively large and the peak magnitude of the forward energy flux at small λ_z near the wall is relatively small.

The spanwise interscale fluxes of the Reynolds shear stress Tr^z_{-uv} and the turbulent heat flux $Tr^z_{-v\theta}$ are also presented in Figure 6. As shown in the panel (a), the Reynolds shear stress flux Tr^z_{-uv} indicates, interestingly, the backward transfers throughout the channel, as first experimentally observed by Kawata and Alfredsson [1]. This is in contrast to the turbulent energy transfer Tr^z_{uu}, which mainly indicates forward transfers throughout the channel except for the near-wall region. Such inverse interscale transport of the Reynolds shear stress has also been reported in turbulent channel [11] and boundary-layer [5] flows.
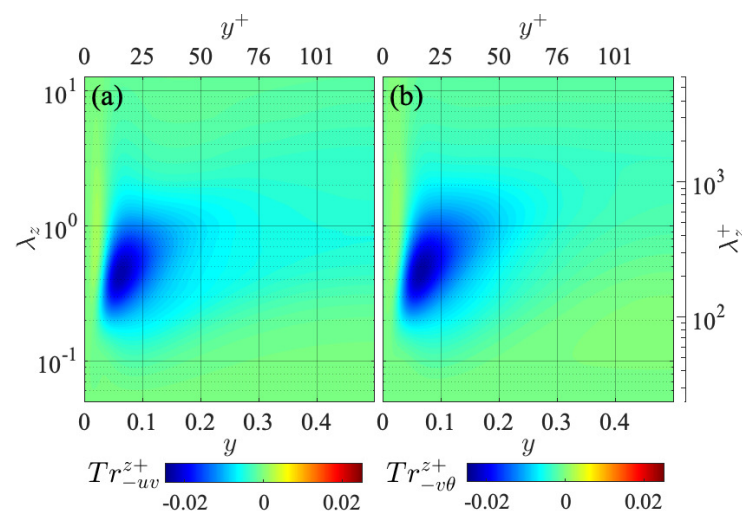

Figure 6. Spanwise interscale fluxes of (**a**) Reynolds shear stress Tr^z_{-uv} and (**b**) turbulent heat flux $Tr^z_{-v\theta}$, presented in the same manner as in Figure 5.

The interscale transfer of the turbulent heat flux $Tr^z_{-v\theta}$ gives a similar distribution to that of Tr^z_{-uv}, as presented in Figure 6b. The difference between the distributions of

these spanwise interscale fluxes is that $Tr^z_{-v\theta}$ spans to slightly larger spanwise wavelengths than Tr^z_{-uv}. While it is still unclear what physical phenomenon is represented by such an inverse interscale transfer of $-\langle uv \rangle$ and $-\langle v\theta \rangle$, the similar distributions of Tr^z_{-uv} and $Tr^z_{-v\theta}$ indicate a close analogy between the transport of the Reynolds shear stress and turbulent heat flux.

3.3. Spectra of Spatial Turbulent Fluxes of the Reynolds Stresses and Temperature-Related Statistics

We focus on the spatial turbulent transport of the Reynolds stresses and temperature-related statistics. Figure 7 presents the profiles of the triple velocity correlations $\langle u^2v \rangle$ and $-\langle uv^2 \rangle$ and those of the triple velocity-temperature correlations $\langle \theta^2v \rangle$ and $-\langle v^2\theta \rangle$. As for the physical interpretations of these third-order statistics, $\langle u^2v \rangle$ and $\langle \theta^2v \rangle$ represent, respectively, the wall-normal spatial fluxes of the velocity fluctuation $\langle u^2 \rangle$ and the temperature fluctuation $\langle \theta^2 \rangle$, which are caused by turbulent fluid motions. Similarly, $-\langle uv^2 \rangle$ and $-\langle v^2\theta \rangle$ indicate the turbulent spatial fluxes of the Reynolds shear stress $-\langle uv \rangle$ and the turbulent heat transfer $-\langle v\theta \rangle$, respectively. As discussed in Section 2.2, these third-order statistics represent the spatial transport effect caused by interactions between different scales. As shown in Figure 7, the profiles of the triple correlations are all qualitatively similar, indicating transport further towards the wall in the near-wall region and transport towards the channel centre in the far-wall region.
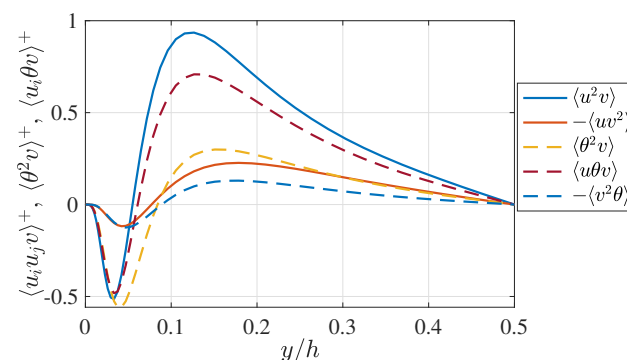

Figure 7. Profiles of the velocity triple correlations $\langle u^2v \rangle$ and $-\langle uv^2 \rangle$ and the temperature-velocity triple correlations $\langle \theta^2v \rangle$ and $-\langle v^2\theta \rangle$. The values are scaled by u_τ^3, $u_\tau T_\tau^2$, or $u_\tau^2 T_\tau$.

Figure 8 presents the distributions of the spanwise one-dimensional spectra of the turbulent energy transports E^z_{uuv}, $E^z_{\theta\theta v}$, and $E^z_{u\theta v}$ in the premultiplied form. These spectra represent the spectral contents of the triple correlations $\langle u^2v \rangle$, $\langle \theta^2v \rangle$, and $\langle u\theta v \rangle$ presented in Figure 7. As shown in Figure 8, these spectra of spatial energy fluxes show similar distributions, indicating that the negative (i.e., towards the wall) spatial transport in the near-wall region mainly occurs at the largest wavelength $\lambda_z/h \approx 2.5$, while the positive (towards the channel centre) transport occurs at two smaller scales: the middle scale roughly at $\lambda_z/h \approx 0.8$ and relatively small wavelengths around $\lambda_z/h \approx 0.2$ ($\lambda_z^+ \approx 50$). As the wavelength of the negative $k_z E^z_{uuv}$ peak at the largest scale $\lambda_z/h = 2.5$ coincides with the typical spanwise spacing of u-streaks of the very-large-scale structure, the large-scale negative peak presumably represents the turbulence transports in which the fluctuating velocities and temperature are carried towards the wall vicinity by the secondary fluid motions of the very-large-scale structures. As for the positive $k_z E^z_{uuv}$ peak at a relatively small scale $\lambda_z^+ \approx 50$, this wavelength fairly matches the peak location of the premultiplied wall-normal turbulent energy spectrum $k_z E^z_{vv}$ in the near-wall region [27], which is likely related to the coherent fluid motions in the near-wall region. Therefore, it can be inferred that this positive $k_z E^z_{uuv}$ peak indicates the turbulent energy transport driven by the wall-normal fluid motions by the near-wall coherent structures. On the other hand, the wavelength of the positive $k_z E^z_{uuv}$ peak on the larger-scale side, $\lambda_z/h \approx 0.8$ ($\lambda_z^+ \approx 100$), is on the order of the full channel height h, but any corresponding characteristic length scale of coherent fluid motion is not found. As this scale lies in the middle wavelength range between the

length scales of the very-large-scale and near-wall structures, this positive $k_z E_{uuv}^z$ peak may represent the energy transport caused by interactions between these inner and outer coherent structures.
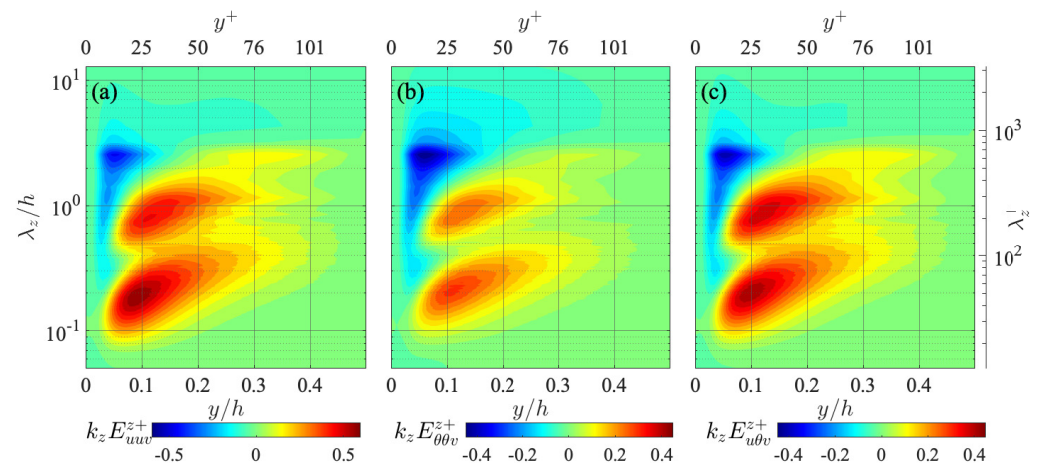

Figure 8. Spanwise one-dimensional premultiplied spectra of turbulent spatial fluxes of (**a**) streamwise turbulent energy $k_z E_{uuv}^z$, (**b**) temperature fluctuation $k_z E_{\theta\theta v}^z$, and (**c**) temperature-velocity correlation $k_z E_{u\theta v}^z$, presented in the same manner as in Figure 3. The values are scaled by u_τ^3, $u_\tau T_\tau^2$, and $u_\tau^2 T_\tau$, respectively.

Figure 9 presents the distributions of the spatial flux spectra of the Reynolds shear stress E_{-uvv}^z and the turbulent heat transfer $E_{-v\theta v}^z$. Similarly to other spatial flux spectra presented in Figure 8, E_{-uvv}^z and $E_{-v\theta v}^z$ are the spectral contents of the triple correlations $-\langle uv^2 \rangle$ and $-\langle v^2\theta \rangle$ presented in Figure 7, indicating the wall-normal fluxes of the Reynolds shear stress $-\langle uv \rangle$ and the turbulent heat flux $-\langle v\theta \rangle$ at each wavelength λ_z, respectively. As shown in the figure, these spatial flux spectra of the cross correlations present qualitatively similar distributions to those of the spatial turbulent energy fluxes, such as E_{uuv}^z and $E_{\theta\theta v}^z$ presented in Figure 8, indicating the peak of negative transport at the largest wavelength $\lambda_z/h \approx 2.5$ near the wall, and the positive transport peaks at two smaller wavelengths in the relatively far-wall region. This tendency is in contrast to the interscale fluxes in that the interscale fluxes of the cross correlations Tr_{-uv}^z and $Tr_{-v\theta}^z$ show clearly different behaviours from those of turbulent energies such as Tr_{uu}^z and $Tr_{\theta\theta}^z$, as observed in Figures 5 and 6.
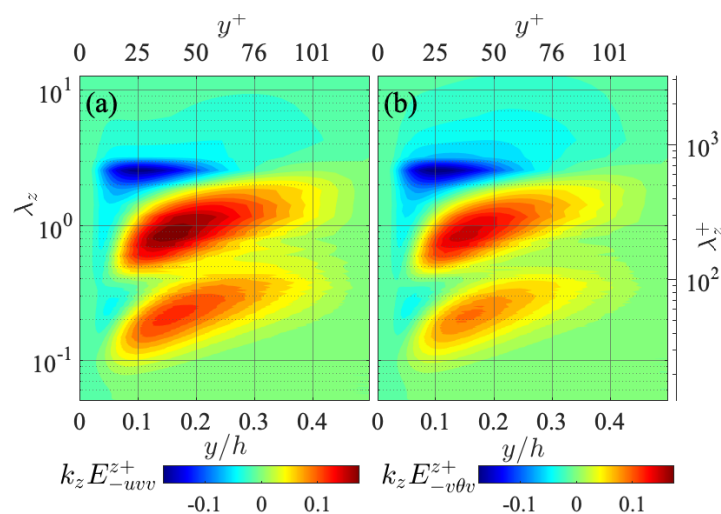

Figure 9. Spanwise one-dimensional premultiplied spectra of turbulent spatial fluxes of (**a**) Reynolds shear stress E_{-uvv}^z and (**b**) the turbulent heat flux $E_{-v\theta v}^z$, presented in the same manner as in Figure 3. The values are scaled by u_τ^3 and $u_\tau^2 T_\tau$, respectively.

As described so far, the spectral distributions of the fluctuating velocity and temperature fields have been investigated with respect to their interscale and spatial fluxes, and it has been observed that the temperature-related statistics essentially show similar distributions to the corresponding turbulence statistics, indicating a close similarity between the fluctuating velocity and temperature fields. In the next section, the spectral budgets of the transport equations of the temperature-related statistics are investigated further in detail.

3.4. Budget Analysis of Spectral Transport Equations

Now, we investigate the transport budget of the temperature-related spectra $E_{\theta\theta}^z$, $E_{u\theta}^z$, and $E_{-v\theta}^z$ in detail. The transport budgets of the Reynolds stress spectra are also given in Apendix A and compared to these temperature-related spectra transport when necessary for discussion. Figure 10 presents the distributions of terms in the transport equation of the temperature fluctuation spectrum $E_{\theta\theta}^z$:

$$\left(\frac{\partial}{\partial t} + U_k\frac{\partial}{\partial x_k}\right)E_{\theta\theta}^z = pr_{\theta\theta}^z - \xi_{\theta\theta}^z + d_{\theta\theta}^{v,z} + d_{\theta\theta}^{t,z} + tr_{\theta\theta}^z. \tag{38}$$

As shown in the top-left panel, the temperature fluctuation is produced by $pr_{\theta\theta}^z$ mainly at a relatively small wavelength of $\lambda_z^+ \approx 100$ in the near-wall region, which roughly corresponds to the y-position and the spanwise length scale of the coherent structure in the near-wall region. This tendency is quite similar to the distribution of the streamwise turbulent energy production spectrum pr_{uu}^z given in Figure A1, see Appendix A. The similarity between these productions can be understood by noting that $pr_{\theta\theta}^z$ and pr_{uu}^z depend on the cospectra $E_{-v\theta}^z$ and E_{-uv}^z, respectively, as

$$pr_{\theta\theta}^z = E_{-v\theta}^z\frac{\mathrm{d}\Theta}{\mathrm{d}y}, \quad pr_{uu}^z = E_{-uv}^z\frac{\mathrm{d}U}{\mathrm{d}y}, \tag{39}$$

and the distributions of $E_{-v\theta}^z$ and E_{-uv}^z and the profiles of U and Θ are similar to each other, respectively, as presented in Figures 1 and 4.
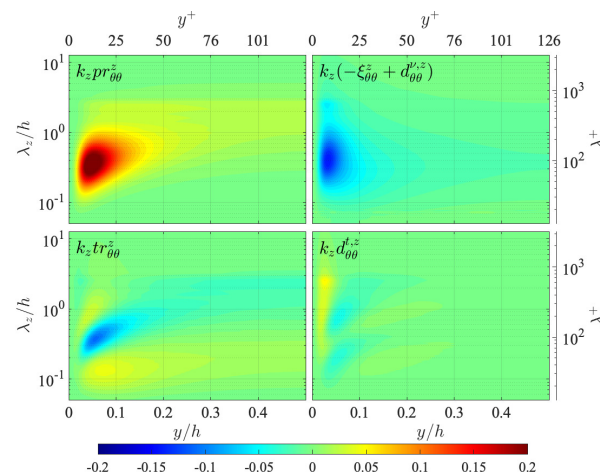

Figure 10. Space-wavelength ($y - \lambda_z$) diagrams of terms in the transport equation of the temperature fluctuation spectrum $E_{\theta\theta}^z$: (**top left**) production $pr_{\theta\theta}^z$; (**top right**) viscous terms $\xi_{\theta\theta}^z + d_{\theta\theta}^{v,z}$; (**bottom left**) interscale transport $tr_{\theta\theta}^z$; (**bottom right**) turbulent diffusion $d_{\theta\theta}^{t,z}$. The terms are presented in the premultiplied form, and the values are scaled by $u_\tau^2 T_\tau^2/\nu$.

The distribution of the interscale transport $tr_{\theta\theta}^z$ presents the consequential energy gain/loss by the interscale energy flux $Tr_{\theta\theta}^z$ shown in Figure 5 as $tr_{\theta\theta}^z = -\partial Tr_{\theta\theta}^z/\partial k_z$, and it is shown in Figure 10 that the energy is removed from the region around the peak of $pr_{\theta\theta}^z$ and transported towards both larger and smaller λ_z ranges in the near-wall region by the interscale energy transport $tr_{\theta\theta}^z$, while in the channel-core region, the energy is mainly transported in the forward direction from around $\lambda_z/h \approx 2.5$ to a smaller λ_z range.

The distribution of the spectral turbulent diffusion $d_{\theta\theta}^{t,z}$ represents the energy gain/loss by the turbulent spatial flux $E_{\theta\theta v}^z$ presented in Figure 8, as $d_{\theta\theta}^{t,z} = -\partial E_{\theta\theta v}^z/\partial y$. Its contribution is relatively small as compared to the other terms, but it can be seen that the energy is supplied to the wall vicinity at a large wavelength $\lambda_z/h \approx 2.5$, and the energy transport towards the channel central region is also observed at two relatively small wavelength ranges, corresponding to the distribution of the turbulent spatial flux $E_{\theta\theta v}^z$. The energy produced by $pr_{\theta\theta}^z$ and transported by $tr_{\theta\theta}^z$ and $d_{\theta\theta}^{t,z}$ is eventually dissipated by the viscous dissipation $\xi_{\theta\theta}^z$. Such distributions of the terms in the $E_{\theta\theta}^z$ transport equation described above are quite similar to those of the corresponding terms in the E_{uu}^z transport equation given in Figure A1.

The clear difference between the transport equations of the temperature fluctuation spectrum $E_{\theta\theta}^z$ and the streamwise turbulent energy E_{uu}^z is that no pressure-related term exists in the $E_{\theta\theta}^z$ transport equation, whereas in the E_{uu}^z transport, the pressure-strain cospectrum π_{uu}^z plays an important role in redistributing energy from E_{uu}^z to other components of turbulent energy spectra. Despite such a distinct difference, the distributions of the terms in the $E_{\theta\theta}^z$ equation are quite similar to those of the corresponding terms of the E_{uu}^z transport equation (compare Figures 10 and A1). In the following, the budget balances of the $E_{\theta\theta}^z$ and E_{uu}^z equations are compared in more detail.

Figure 11 presents a detailed balance between the terms of the $E_{\theta\theta}^z$ and E_{uu}^z equations at a near-wall location $y^+ = 16$ and the quarter height of the channel $y/h = 0.25$ ($y^+ \approx 60$). The values are scaled by the maximum value of each production term. As shown in the panel (a), the profiles of the production, interscale transport, and turbulent diffusion of the $E_{\theta\theta}^z$ and E_{uu}^z transport equations show a good collapse in the near-wall region. The production terms indicate a significant energy gain at $\lambda_z^+ \approx 100$, as already pointed out above, and the interscale transport terms are shown to transfer the energy from this energy-producing wavelength to both larger and smaller λ_z ranges, where the turbulent diffusion terms transfer some energy to other y-positions. As previously mentioned, there is no term in the $E_{\theta\theta}^z$ transport budget corresponding to the pressure-strain term π_{uu}^z in the E_{uu}^z transport, and the consequential difference between the budget balances of the $E_{\theta\theta}^z$ and E_{uu}^z transport equation is mainly manifested by the viscous terms. As there is no energy absorption by the pressure-strain cospectrum in the $E_{\theta\theta}^z$ budget, the viscous terms $\xi_{\theta\theta}^z + d_{\theta\theta}^{v,z}$ show a clearly larger contribution than $\xi_{uu}^z + d_{uu}^{v,z}$ to compensate for the absence of the pressure term and, thus, the transport equation is balanced.

At the quarter height of the channel $y/h = 0.25$, as shown in Figure 11b, the profiles of the production terms collapse similarly to those in the near-wall region, but the λ_z range where energy is dissipated by viscosity is significantly smaller than the energy-producing λ_z range. Hence, the interscale transport terms bridge these energy-producing and -dissipating λ_z ranges by forward energy transfer and do not exhibit reversed energy transfer, unlike in the near-wall region. It is also observed that the production terms present not only the largest peak of energy gain at $\lambda_z^+ \approx 200$ but also a secondary peak at $\lambda_z/h \approx 2.5$, which corresponds to the very-large-scale structures. The turbulent diffusion terms present energy gains at two wavelength ranges, which represents energy supply from the near-wall region (see the $d_{\theta\theta}^{t,z}$ and $d_{uu}^{t,z}$ distributions in Figures 10 and A1). The contribution of the pressure-strain correlation π_{uu}^z in the E_{uu}^z transport equation is relatively large compared to that in the near-wall location shown in the panel (a), and the interscale transport $tr_{\theta\theta}^z$ as well as the viscous terms $\xi_{\theta\theta}^z + d_{\theta\theta}^{v,z}$ show significantly larger contributions than the counterparts in the E_{uu}^z equation to compensate for the absence of the energy absorption by π_{uu}^z. Thus, both in the near- and far-wall regions of the channel, the energy productions in the $E_{\theta\theta}^z$ and E_{uu}^z transports are quite similar to each other, but more energy is dissipated by the viscous terms in the $E_{\theta\theta}^z$ transport, compensating for the absence of the energy loss by the pressure-related term.
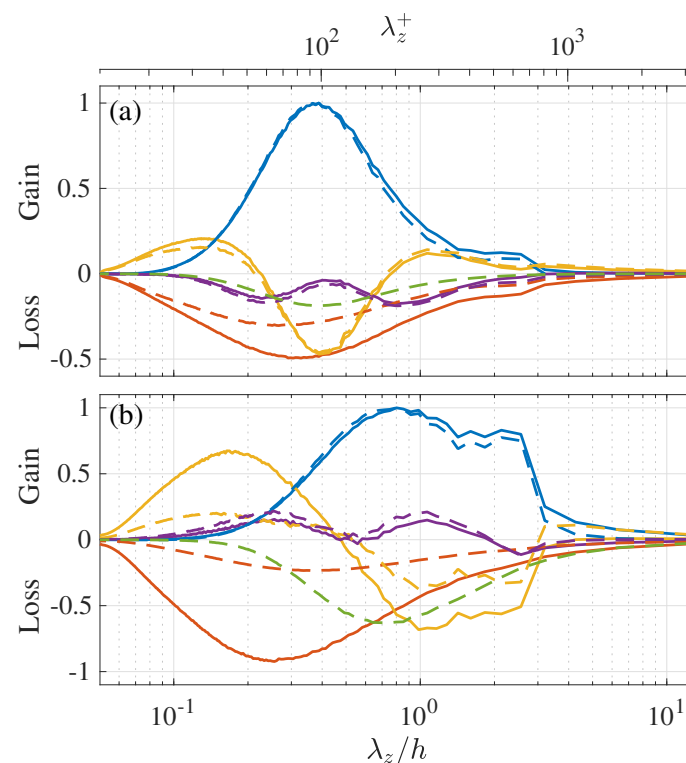
Figure 11. Detailed budget balance of the $E_{\theta\theta}^z$ and E_{uu}^z transport equation at (**a**) a near-wall location $y^+ = 16$ and (**b**) the quarter height of the channel $y/h = 0.25$: (blue) production; (red) viscous dissipation+viscous diffusion; (yellow) interscale transport; (purple) turbulent diffusion; (light green) pressure-strain cospectrum π_{uu}^z. The solid and dashed lines represent terms in the $E_{\theta\theta}^z$ and E_{uu}^z equations, respectively. The terms are given in the premultiplied form, and the values are scaled by the peak value of each production term.

The transport equation of the velocity-temperature cospectrum $E_{u\theta}^z$ is written as

$$\left(\frac{\partial}{\partial t} + U_k \frac{\partial}{\partial x_k}\right) E_{u\theta}^z = pr_{u\theta}^z - \xi_{u\theta}^z + d_{u\theta}^{\nu,z} + \phi_{u\theta}^z + d_{u\theta}^{t,z} + tr_{u\theta}^z, \tag{40}$$

and the distributions of the terms in the right-hand side are presented in Figure 12. It is clearly seen here that the $E_{u\theta}^z$ transport equation has a pressure term $\phi_{u\theta}^z$ and it essentially functions as an energy sink throughout the channel, similarly to the pressure-strain energy redistribution term π_{uu}^z in the E_{uu}^z transport equation. It is also noteworthy that the production of the velocity-temperature cospectrum $pr_{u\theta}^z$ depends on both the Reynolds shear stress spectra E_{-uv}^z and the turbulent heat flux spectra $E_{-v\theta}^z$ as

$$pr_{u\theta}^z = E_{-v\theta}^z \frac{dU}{dy} + E_{-uv}^z \frac{d\Theta}{dy}, \tag{41}$$

unlike the productions of other spectra, such as pr_{uu}^z and $pr_{\theta\theta}^z$, which only depend on either E_{-uv}^z or $E_{-v\theta}^z$. The distribution of $pr_{u\theta}^z$ is, however, similar to those of pr_{uu}^z and $pr_{\theta\theta}^z$, as the distributions of E_{-uv}^z and $E_{-v\theta}^z$ are similar to each other and so are the profiles of U and Θ. Each term of the $E_{u\theta}^z$ transport equation presented in Figure 12 shows a similar distribution to the corresponding term in the E_{uu}^z transport equation shown in Figure A1. Since the $E_{u\theta}^z$ transport equation has a pressure-related term, unlike the $E_{\theta\theta}^z$ equation, the budget balance is even closer to the transport of the streamwise turbulent energy E_{uu}^z than that of the $E_{\theta\theta}^z$ transport.
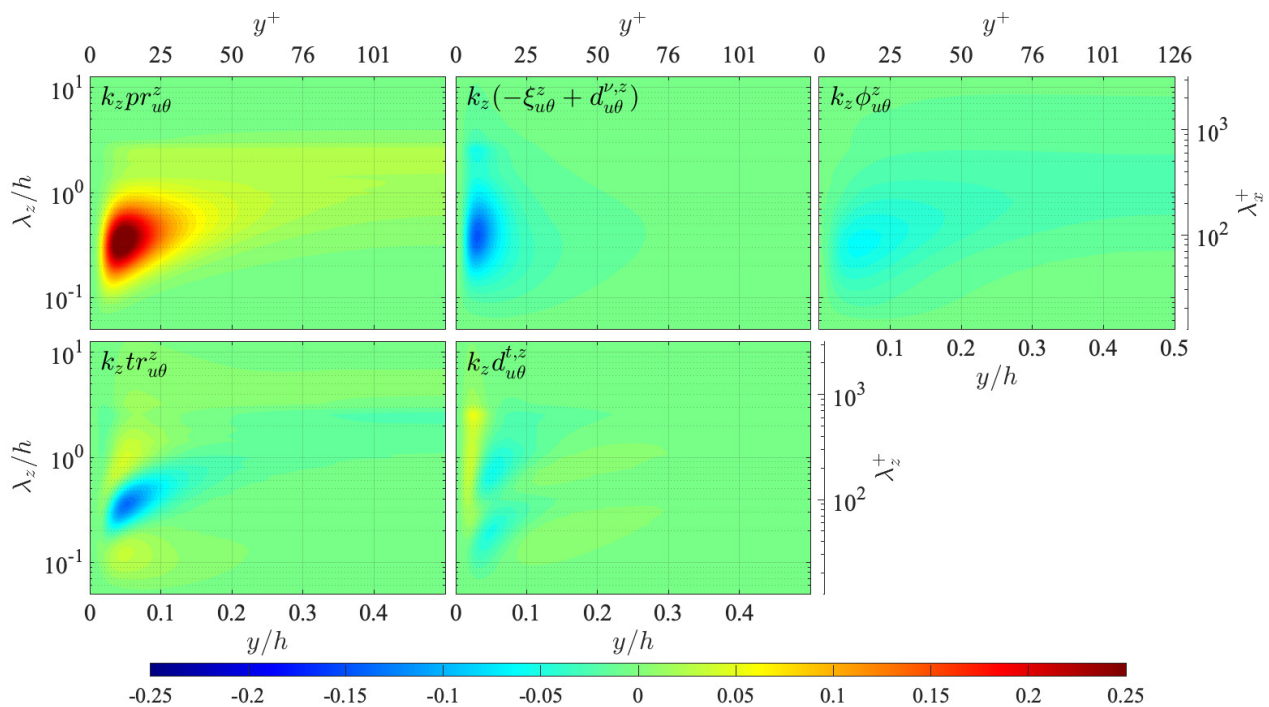
Figure 12. Distribution of terms in the transport equation of the velocity-temperature cospectrum $E_{u\theta}^z$ presented in the same manner as in Figure 10: (**top left**) production $pr_{u\theta}^z$; (**top centre**) viscous terms $\xi_{u\theta}^z + d_{u\theta}^{\nu,z}$; (**top right**) pressure term $\phi_{u\theta}^z$; (**bottom right**) interscale transport $tr_{u\theta}^z$; (**bottom centre**) turbulent diffusion $d_{u\theta}^{t,z}$. The terms are presented in the premultiplied form, and the values are scaled by $u_\tau^3 T_\tau / \nu$.

Now, we shed light on the transport of the turbulent heat flux spectrum $E_{-v\theta}^z$. The transport equation of $E_{-v\theta}^z$ is written as

$$\left(\frac{\partial}{\partial t} + U_k \frac{\partial}{\partial x_k}\right) E_{-v\theta}^z = pr_{-v\theta}^z - \xi_{-v\theta}^z + d_{-v\theta}^{\nu,z} + \phi_{-v\theta}^z + d_{-v\theta}^{t,z} + tr_{-v\theta}^z, \quad (42)$$

and the distributions of the terms on the right-hand side are presented in Figure 13. As shown here, $E_{-v\theta}^z$ is produced by the production term $pr_{-v\theta}^z$ mainly in the near-wall region at wavelengths around $\lambda_z^+ \approx 100$, similarly to the other energy spectra $pr_{\theta\theta}^z$ and $pr_{u\theta}^z$. The energy gain by the production $pr_{-v\theta}^z$ is mainly balanced by the pressure term $\phi_{-v\theta}^z$, and the viscous terms do not play an important role.

The turbulent transport terms $tr_{-v\theta}^z$ and $d_{-v\theta}^{t,z}$ are shown to partly transport $E_{-v\theta}^z$ in scale and space, respectively. The interscale transport $tr_{-v\theta}^z$ presents the energy gain/loss by the inverse interscale flux $Tr_{-v\theta}^z$ investigated in Figure 6, and the distribution shows that the turbulent heat flux $-\langle v\theta \rangle$ is mainly transported from wavelengths around $\lambda_z/h \approx 0.25$ ($\lambda_z^+ \approx 65$) to a larger λ_z range around $\lambda_z/h \approx 0.75$ ($\lambda_z^+ \approx 190$) in the near-wall region. The distribution of $d_{-v\theta}^{t,z}$ indicates weak spatial transports similarly to $d_{\theta\theta}^{t,z}$ and $d_{u\theta}^{t,z}$, where $-\langle v\theta \rangle$ is supplied to the wall vicinity from the channel-core region at the largest wavelengths $\lambda_z/h \approx 2.5$, and at a smaller λ_z range, $-\langle v\theta \rangle$ is transported from the near- to far-wall region at two different wavelengths.
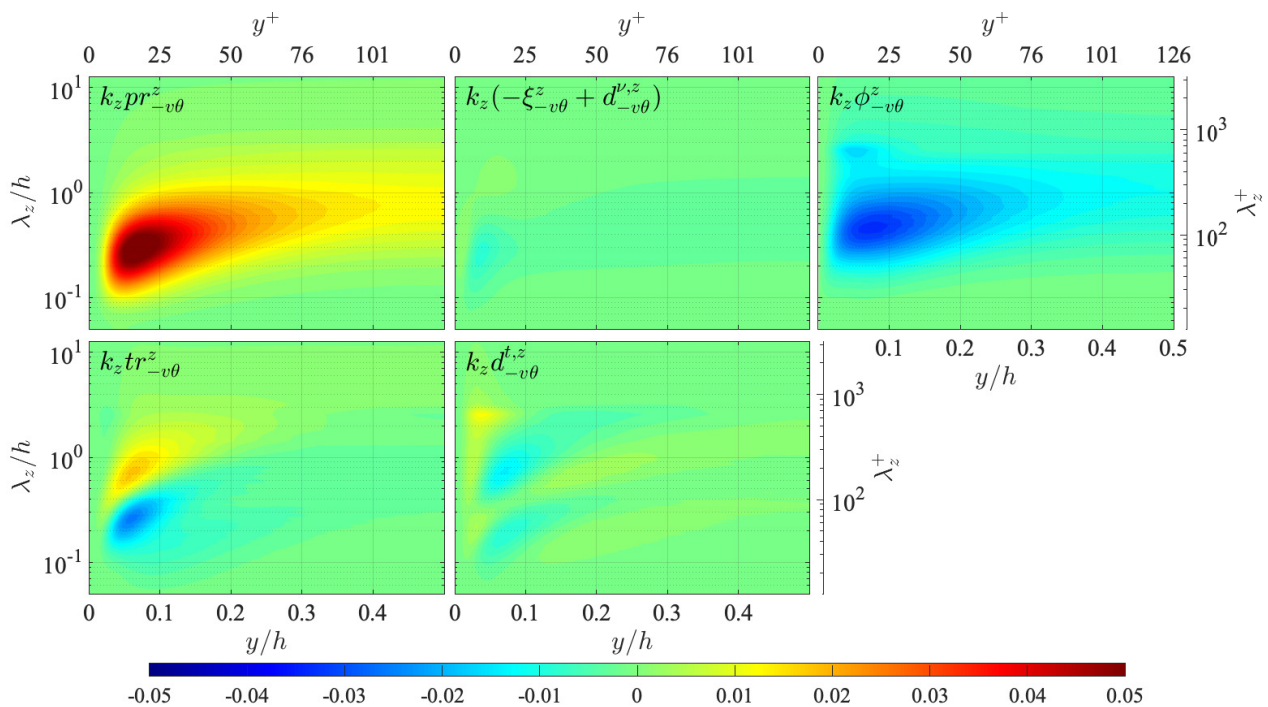
Figure 13. Distribution of terms in the transport equation of the turbulent heat flux spectrum $E^z_{-v\theta}$ presented in the same manner as in Figure 12: (**top left**) production $pr^z_{-v\theta}$; (**top centre**) viscous terms $\xi^z_{-v\theta} + d^{\nu,z}_{-v\theta}$; (**top right**) pressure term $\phi^z_{-v\theta}$; (**bottom left**) interscale transport $tr^z_{-v\theta}$; (**bottom centre**) turbulent diffusion $d^{t,z}_{-v\theta}$. The terms are presented in the premultiplied form, and the values are scaled by $u^3_\tau T_\tau / \nu$.

The tendencies of the terms in the $E^z_{-v\theta}$ transport equation described above are quite similar to those of the corresponding terms in the transport equation of the Reynolds shear stress spectrum E^z_{-uv}, as can be seen by comparing Figure 13 in Figure A4 in Appendix A. It is particularly noteworthy here that the productions of $E^z_{-v\theta}$ and E^z_{-uv} are both dependent on the wall-normal turbulent energy spectrum E^z_{vv} as

$$pr^z_{-v\theta} = E^z_{vv} \frac{\mathrm{d}\Theta}{\mathrm{d}y}, \quad pr^z_{-uv} = E^z_{vv} \frac{\mathrm{d}U}{\mathrm{d}y}, \tag{43}$$

which indicates that the Reynolds shear stress $-\langle uv \rangle$ and the turbulent heat flux $-\langle v\theta \rangle$ are produced at the same scale.

Figure 14 presents a detailed comparison of the transport budgets of $E^z_{-v\theta}$ and E^z_{-uv} at a near-wall location $y^+ = 16$ and the quarter height of the channel in the same manner as in Figure 11. Note here that in both panels the profiles of the productions $pr^z_{-v\theta}$ and pr^z_{-uv} are exactly on top of each other since their profiles are similar, as shown by Equation (43). As shown here, at both wall-normal locations, the spectral budget balances of the $E^z_{-v\theta}$ and E^z_{-uv} transport are quite similar to each other. It is also shown at both wall-normal locations that the peaks of the pressure terms are located at a larger λ_z than those of the production terms in both $E^z_{-v\theta}$ and E^z_{-uv} transport, which indicates that the turbulent heat flux $-\langle v\theta \rangle$ and the Reynolds shear stress $-\langle uv \rangle$ are dissipated by the effect of pressure at larger spanwise wavelengths than those at which they are produced by the mean temperature or velocity gradients. Such tendencies are in contrast to the transport of the energy spectra such as E^z_{uu} and $E^z_{\theta\theta}$, where the energy is dissipated basically at smaller scales than produced. This is attributable to the contribution of the interscale transport terms $tr^z_{-v\theta}$ and tr^z_{-uv} to transport the energy from smaller to larger scales.
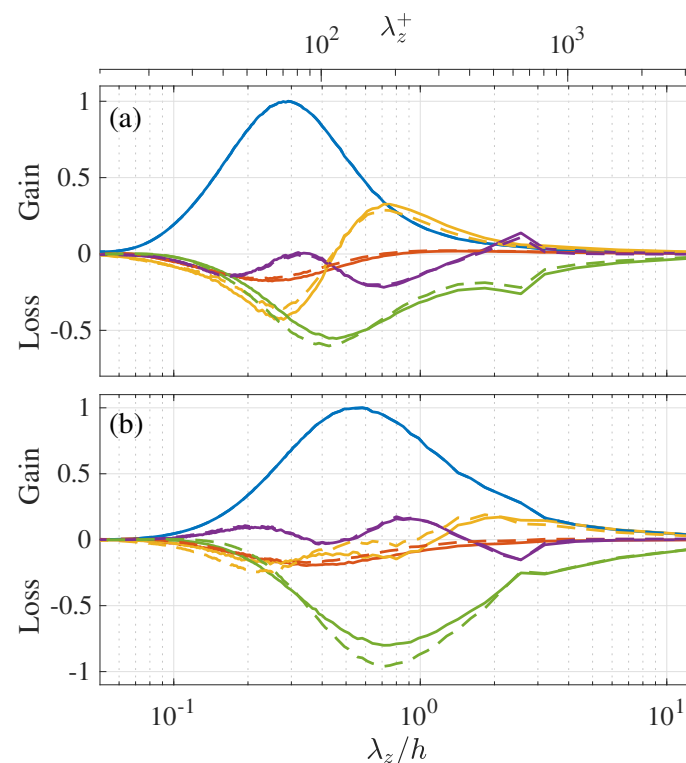
Figure 14. Detailed budget balance of the $E^z_{-v\theta}$ and E^z_{-uv} transport equation at (**a**) a near-wall location $y^+ = 16$ and (**b**) the quarter height of the channel $y/h = 0.25$ presented in the same manner as in Figure 11: (blue) production; (red) viscous dissipation+viscous diffusion; (yellow) interscale transport; (purple) turbulent diffusion; (light green) pressure term.

It is interesting to note that the agreements between the turbulent diffusion terms $d^{t,z}_{-v\theta}$ and $d^{t,z}_{-uv}$ are particularly good, while a slight difference can be found between the interscale transport terms $tr^z_{-v\theta}$ and tr^z_{-uv}, although both the turbulent diffusion and interscale transport represent the transport effect caused by nonlinear interactions between different scales. Such good agreement between the turbulent diffusion terms are also observed between the $E^z_{\theta\theta}$ and E^z_{uu} transports, as already pointed out in Figure 11.

4. Discussion and Concluding Remarks

In the previous section, the spectral budgets of the temperature-related spectra, such as $E^z_{\theta\theta}$, $E^z_{u\theta}$, and $E^z_{-v\theta}$, were compared with those of the corresponding Reynolds stress spectra, E^z_{uu} and E^z_{-uv}, and a close analogy between those turbulence transports was indicated. Of particular interest is the close similarity between the spectral transports of the Reynolds shear stress $-\langle uv \rangle$ and the turbulent heat flux $-\langle v\theta \rangle$, where inverse interscale transport from a smaller to larger λ_z is observed.

The turbulent diffusion and interscale transport are two different aspects of nonlinear multi-scale interactions of turbulence, and the physical phenomena these spatial and interscale transport terms represent is of great interest. As shown in Figure 14a, the turbulent diffusions $d^{t,z}_{-v\theta}$ and $d^{t,z}_{-uv}$ are shown to remove energy from the near-wall location in two λ_z ranges around $\lambda^+_z \approx 50$ and 180, and the removed $-\langle v\theta \rangle$ and $-\langle uv \rangle$ are partly transported towards the central region of the channel, as indicated by the profiles of $d^{t,z}_{-v\theta}$ and $d^{t,z}_{-uv}$ at $y/h = 0.25$ given in Figure 14b. In particular, the energy gains by $d^{t,z}_{-v\theta}$ and $d^{t,z}_{-uv}$ at $y/h = 0.25$ are shown to balance well with the energy loss by the interscale energy transport $tr^z_{-v\theta}$ and tr^z_{-uv}, which suggests that the energy ($-\langle v\theta \rangle$ and $-\langle uv \rangle$) spatially transferred from the near-wall region to this wall-normal location at relatively small λ_z is further transferred to a larger λ_z range. Kawata and Alfredsson [1] experimentally observed similar Reynolds shear stress transport from smaller λ_z near the wall to larger λ_z in the

channel-core region in turbulent plane Couette flow and conjectured that it may represent the influences of the near-wall smaller-scale coherent structures on the very-large-scale structures, which is similar to the concept of a co-supporting cycle of the inner and outer structures proposed by Toh and Itano [34].

It should be mentioned here that the inverse interscale transport of the Reynolds shear stress and turbulent heat flux described so far are observed based on one-dimensional spanwise-Fourier-mode analysis, and therefore, the interscale energy transfer in the streamwise length scales is not investigated. In fact, such reversed interscale transfers are not observed by the analysis based on the streamwise Fourier modes. In a numerical simulation by Kawata and Tsukahara [4], spectral budget analysis was performed based on both one-dimensional streamwise and spanwise Fourier modes, and it was shown that the interscale transfers of the turbulent energy and Reynolds shear stress in the streamwise wavenumber direction are basically forward transfers (i.e., from larger to smaller scales). Lee and Moser [7] performed two-dimensional Fourier-mode analysis on the turbulent energy transport and showed that the energy transport between wavenumbers with the same magnitude but different directions, which may not represent energy transfer between really different length scales, can be observed as inverse interscale energy transfers through one-dimensional Fourier mode analysis. These observations suggest that the inverse energy transfers in the spanwise length scales may not simply be interpreted as interaction from smaller- to larger-scale structures.

Some recent studies, on the other hand, investigated the relationship between the inner-outer interaction in wall turbulence and the inverse interscale energy transfers in the spanwise length scales in detail. Doohan et al. [3] investigated the interactions between self-sustaining processes (SSPs) of coherent structures near and away from the wall and argued that the energy transfer from the smaller-scale SSP leads to the formation of the wall-reaching part of streaks of the larger-scale SSP. Chiarini et al. [11] also investigated spatial and interscale energy fluxes by analysing the anisotropic generalised Kolmogorov equation taking into account both the streamwise and spanwise length scale and observed some energy paths from smaller scales near the wall to larger scales away from the wall. Chan et al. [5] also observed the inverse interscale transport of the Reynolds shear stress in a turbulent boundary layer, and based on a detailed quadrant analysis, they interpreted it as the net energy transfer from the small-scale ejection (Q2) and sweep (Q4) events to their large-scale counterparts. Thus, what the inverse interscale energy transports in the spanwise lengths scales is still a subject of intense debate. Nevertheless, the transport of the turbulent heat flux spectrum $E^z_{-v\theta}$ is found to be quite similar to that of the Reynolds shear stress spectrum E^z_{-uv}, which indicates a close scale-by-scale similarity between the turbulent momentum and heat transfers.

In the present study, the transport budgets of temperature-related spectra, such as the temperature-variance and turbulent heat flux spectra, were investigated in turbulent plane Couette flow with a passive-scalar heat transfer at the Reynolds number $Re_\tau = 126$ and the Prandtl number $Pr = 0.71$ based on DNS data. It was found that the transport budgets of the temperature-related spectra present quite similar tendencies to those of the corresponding Reynolds stress spectra, including the spectral transport of the Reynolds shear stress and turbulent heat flux, where inverse interscale transfers are observed throughout the channel. It is also noteworthy that the distributions of the spatial flux spectra are all similar, regardless of the spatial fluxes of turbulent energies such as $\langle u^2 \rangle$ and $\langle \theta^2 \rangle$ or those of cross correlations such as $-\langle uv \rangle$ and $-\langle v\theta \rangle$. This is in contrast to how the interscale fluxes of $-\langle uv \rangle$ and $-\langle v\theta \rangle$ exhibit notably different behaviours from those of turbulent energies such as $\langle u^2 \rangle$ and $\langle \theta^2 \rangle$. Our next task is to elucidate what physical phenomena these spatial and interscale turbulence transport represent. The present investigation is limited to single values of the Reynolds and Prandtl number, and therefore, the Reynolds- and Prandtl-number dependency of these interscale and spatial fluxes should also be investigated in future studies.

Nomenclature

E_{ij}^z	Spanwise one-dimensional spectra of $\langle u_i u_j \rangle$
$E_{i\theta}^z$	Spanwise one-dimensional spectra of $\langle u_i \theta \rangle$
E_{uu}^z, E_{vv}^z, E_{ww}^z, E_{-uv}^z, $E_{\theta\theta}^z$, $E_{u\theta}^z$, $E_{-v\theta}^z$	Spanwise one-dimensional spectra of $\langle u^2 \rangle$, $\langle v^2 \rangle$, $\langle w^2 \rangle$, $-\langle uv \rangle$, $\langle \theta^2 \rangle$, $\langle u\theta \rangle$, and $-\langle v\theta \rangle$
E_{ijk}^z	Spanwise one-dimensional spectra of $\langle u_i u_j u_k \rangle$
$E_{i\theta k}^z$	Spanwise one-dimensional spectra of $\langle u_i \theta u_k \rangle$
E_{uuv}^z, E_{-uvv}^z, $E_{\theta\theta v}^z$, $E_{u\theta v}^z$, $E_{-v\theta v}^z$	Spanwise one-dimensional spectra of turbulent spatial fluxes $\langle u^2 v \rangle$, $-\langle uv^2 \rangle$, $\langle \theta^2 v \rangle$, $\langle u\theta v \rangle$, and $-\langle v^2 \theta \rangle$
h	Full channel height
k_z	Spanwise wavenumber
$k_{z,c}$	Cutoff spanwise wavenumber for large- and small-scale decomposition
L_x, L_z	Streamwise and spanwise lengths of computational domain
p	Pressure fluctuation
Pr	Prandtl number defined as $Pr = \nu/\alpha$
Re_w	Reynolds number defined as $Re_w = U_w h/\nu$
Re_τ	Friction Reynolds number defined as $Re_\tau = u_\tau \delta/\nu$
T_t, T_b	Temperature of top and bottom wall
ΔT	Temperature difference between top and bottom wall, $\Delta T = T_t - T_b$
T_τ	Friction temperature defined as $T_\tau = Q_\tau/\rho c_p u_\tau$, where Q_τ and c_p are mean wall heat flux and fluid specific heat at constant pressure, respectively
Tr_{ij}^z	Interscale flux of $\langle u_i u_j \rangle$ in spanwise length scales
Tr_{uu}^z, Tr_{-uv}^z, $Tr_{\theta\theta}^z$, $Tr_{u\theta}^z$, $Tr_{-v\theta}^z$	Interscale flux of $\langle u^2 \rangle$, $-\langle uv \rangle$, $\langle \theta\theta \rangle$, $\langle u\theta \rangle$, $-\langle v\theta \rangle$ in spanwise length scales
U	Mean streamwise velocity
U_w	Translating speed of top wall
u, v, w	Fluctuation of streamwise, wall-normal, and spanwise velocity components
u_i	Fluctuation of velocity component in x_i direction
u_τ	Friction velocity defined as $u_\tau = \sqrt{\tau_w/\rho}$, where τ_w is mean wall shear stress
x, y, z	Axes of the coordinates in the streamwise, wall-normal, and spanwise directions
α	Thermal diffusivity of fluid
δ	Half channel height, i.e., $\delta = h/2$
ν	Kinematic viscosity of fluid
ρ	Density of fluid

Θ, θ	Mean temperature and temperature fluctuation
λ_z	spanwise wavelength, i.e., $\lambda_z = 2\pi/k_z$
$\langle\rangle$	Averaged quantities

Terms in transport equations

P_{ij}, ε_{ij}, Φ_{ij}, D_{ij}^v, D_{ij}^t	Production, viscous dissipation, pressure-gradient, viscous diffusion, and turbulent spatial transport terms in $\langle u_i u_j \rangle$ transport equation
Π_{ij}, D_{ij}^p	Pressure-strain correlation and pressure diffusion terms in $\langle u_i u_j \rangle$ transport equation
$P_{\theta\theta}$, $\varepsilon_{\theta\theta}$, $D_{\theta\theta}^v$, $D_{\theta\theta}^t$	Production, viscous dissipation, viscous diffusion, and turbulent spatial transport terms in $\langle \theta^2 \rangle$ transport equation
$P_{i\theta}$, $\varepsilon_{i\theta}$, $\Phi_{i\theta}$, $D_{i\theta}^v$, $D_{i\theta}^t$	Production, viscous dissipation, pressure-gradient, viscous diffusion, and turbulent spatial transport terms in $\langle u_i \theta \rangle$ transport equation
pr_{ij}^z, ξ_{ij}^z, ϕ_{ij}^z, $d_{ij}^{v,z}$, $d_{ij}^{t,z}$, tr_{ij}^z	Production, viscous dissipation, pressure-gradient, viscous diffusion, turbulent spatial transport, and interscale transport terms in E_{ij}^z transport equation
π_{ij}, d_{ij}^p	Pressure-strain and pressure transport terms in E_{ij}^z transport equation
$pr_{\theta\theta}^z$, $\xi_{\theta\theta}^z$, $d_{\theta\theta}^{v,z}$, $d_{\theta\theta}^{t,z}$, $tr_{\theta\theta}^z$	Production, viscous dissipation, viscous diffusion, turbulent spatial transport, and interscale transport terms in $E_{\theta\theta}^z$ transport equation
$pr_{i\theta}^z$, $\xi_{i\theta}^z$, $\phi_{i\theta}^z$, $d_{i\theta}^{v,z}$, $d_{i\theta}^{t,z}$, $tr_{i\theta}^z$	Production, viscous dissipation, pressure-gradient, viscous diffusion, turbulent spatial transport, and interscale transport terms in $E_{i\theta}^z$ transport equation
$pr_{u\theta}^z$, $\xi_{u\theta}^z$, $\phi_{u\theta}^z$, $d_{u\theta}^{v,z}$, $d_{u\theta}^{t,z}$, $tr_{u\theta}^z$	Production, viscous dissipation, pressure-gradient, viscous diffusion, turbulent spatial transport, and interscale transport terms in $E_{u\theta}^z$ transport equation
$pr_{-v\theta}^z$, $\xi_{-v\theta}^z$, $\phi_{-v\theta}^z$, $d_{-v\theta}^{v,z}$, $d_{-v\theta}^{t,z}$, $tr_{-v\theta}^z$	Production, viscous dissipation, pressure-gradient, viscous diffusion, turbulent spatial transport, and interscale transport terms in $E_{-v\theta}^z$ transport equation
pr_{uu}^z, ξ_{uu}^z, π_{uu}^z, $d_{uu}^{v,z}$, $d_{uu}^{t,z}$, tr_{uu}^z	Production, viscous dissipation, pressure-strain, viscous diffusion, turbulent spatial transport, and interscale transport terms in E_{uu}^z transport equation
π_{vv}^z, ξ_{vv}^z, $d_{vv}^{p,z}$, $d_{uu}^{v,z}$, $d_{uu}^{t,z}$, tr_{uu}^z	Pressure-strain, viscous dissipation, pressure transport, viscous diffusion, turbulent spatial transport, and interscale transport terms in E_{vv}^z transport equation
π_{ww}^z, ξ_{vv}^z, $d_{ww}^{v,z}$, $d_{ww}^{t,z}$, tr_{ww}^z	Pressure-strain, viscous dissipation, viscous diffusion, turbulent spatial transport, and interscale transport terms in E_{ww}^z transport equation
pr_{-uv}^z, ξ_{-uv}^z, ϕ_{-uv}^z, $d_{-uv}^{v,z}$, $d_{-uv}^{t,z}$, tr_{-uv}^z	Production, viscous dissipation, pressure-gradient, viscous diffusion, turbulent spatial transport, and interscale transport terms in E_{-uv}^z transport equation

Superscripts

L, S	Large- and small-scale part
$+$	Scaled viscous units, based on ν, u_τ, T_τ

Appendix A. Spectral Budgets of the Reynolds Stress Transports

Here, the transport budgets of the Reynolds stress spectra are presented for comparison to those of the temperature-related spectra given in Figures 10–14. The transport equations of the streamwise turbulent energy E_{uu}^z, wall-normal turbulent energy E_{vv}^z, and spanwise turbulent energy E_{ww}^z are, respectively, written as

$$\left(\frac{\partial}{\partial t} + U_k \frac{\partial}{\partial x_k}\right) E_{uu}^z = pr_{uu}^z - \xi_{uu}^z + d_{uu}^{\nu,z} + \pi_{uu}^z \qquad + d_{uu}^{t,z} + tr_{uu}^z, \tag{A1}$$

$$\left(\frac{\partial}{\partial t} + U_k \frac{\partial}{\partial x_k}\right) E_{vv}^z = \qquad - \xi_{vv}^z + d_{vv}^{\nu,z} + \pi_{vv}^z + d_{vv}^{p,z} + d_{vv}^{t,z} + tr_{vv}^z, \tag{A2}$$

$$\left(\frac{\partial}{\partial t} + U_k \frac{\partial}{\partial x_k}\right) E_{ww}^z = \qquad - \xi_{ww}^z + d_{ww}^{\nu,z} + \pi_{ww}^z \qquad + d_{ww}^{t,z} + tr_{ww}^z, \tag{A3}$$

and the distributions of each term on the right-hand side of these transport equations are given in Figures A1–A3. Among the turbulent energy spectra, only the streamwise component E_{uu}^z has energy production from the mean flow, and the energy sources for the wall-normal and spanwise components E_{vv}^z and E_{ww}^z are the energy redistribution by the pressure-strain cospectra π_{vv}^z and π_{ww}^z, respectively. Note here that

$$\pi_{uu}^z + \pi_{vv}^z + \pi_{ww}^z = 0 \tag{A4}$$

at any y-location and any wavelength λ_z.

The transport equation of the Reynolds shear stress spectrum is

$$\left(\frac{\partial}{\partial t} + U_k \frac{\partial}{\partial x_k}\right) E_{-uv}^z = pr_{-uv}^z - \xi_{-uv}^z + d_{-uv}^{\nu,z} + \phi_{-uv}^z + d_{-uv}^{t,z} + tr_{-uv}^z, \tag{A5}$$

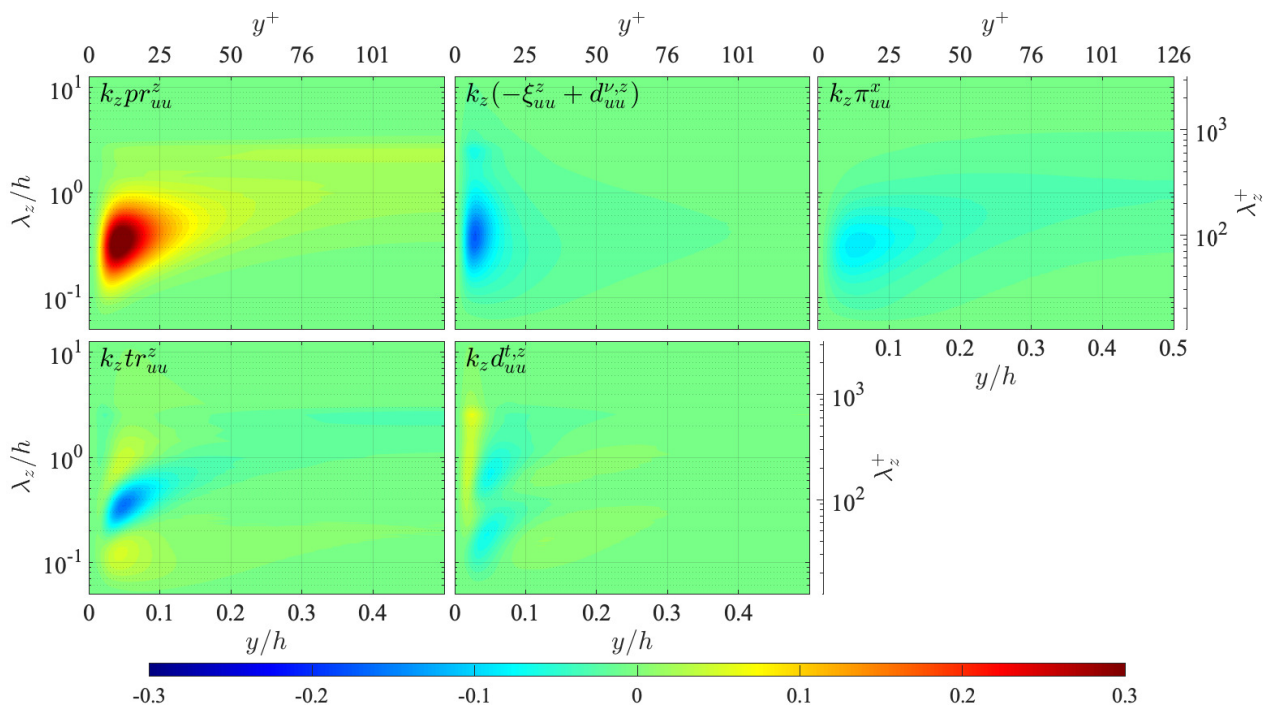and the distributions of the budget terms are shown in Figure A4.

Figure A1. Distribution of terms in the transport equation of the streamwise turbulent energy spectrum E_{uu}^z, presented in the same manner as in Figure 12: (**top left**) production pr_{uu}^z; (**top centre**) viscous terms $\xi_{uu}^z + d_{uu}^{\nu,z}$; (**top right**) pressure-strain energy redistribution π_{uu}^z; (**bottom left**) interscale transport tr_{uu}^z; (**bottom centre**) turbulent diffusion $d_{uu}^{t,z}$. The terms are presented in the premultiplied form, and the values are scaled by u_τ^4/ν.
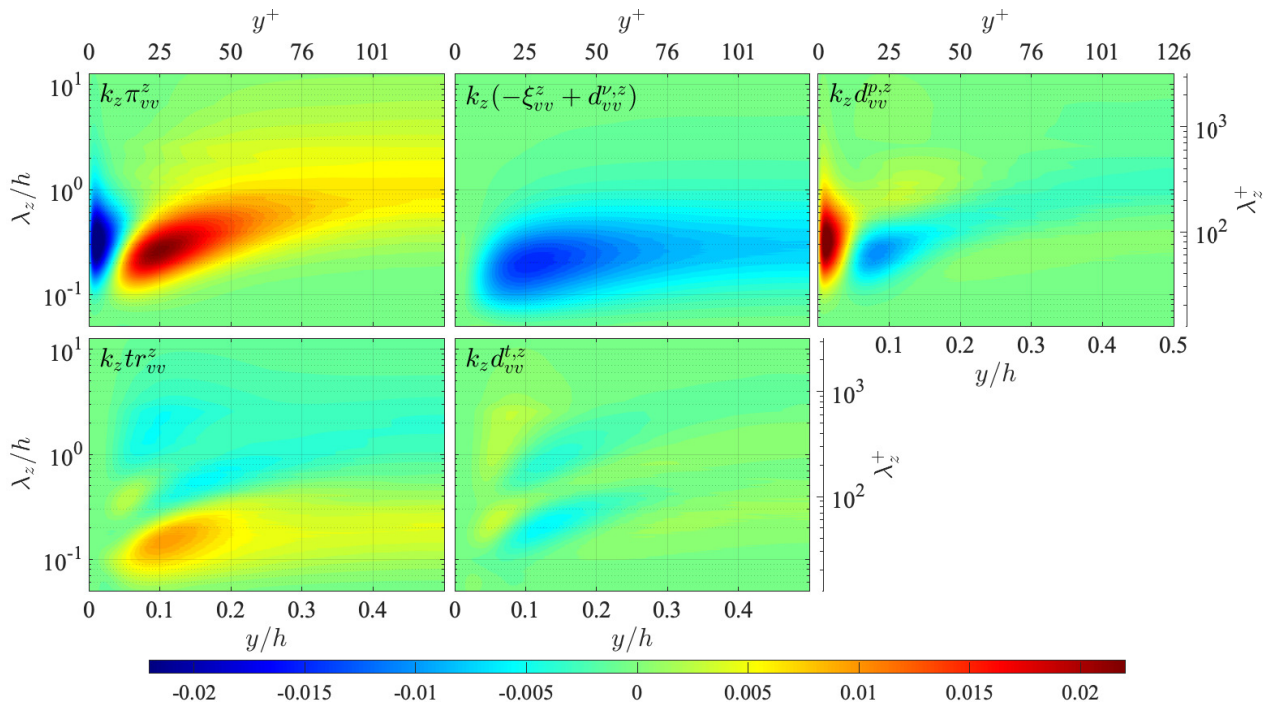
Figure A2. Distribution of terms in the transport equation of the wall-normal turbulent energy spectrum E_{vv}^z, presented in the same manner as in Figure 12: (**top left**) pressure-strain energy redistribution π_{vv}^z; (**top centre**) viscous terms $-\xi_{vv}^z + d_{vv}^{\nu,z}$; (**top right**) pressure diffusion $d_{vv}^{p,z}$; (**bottom left**) interscale transport tr_{vv}^z; (**bottom right**) turbulent diffusion $d_{vv}^{t,z}$. The terms are presented in the premultiplied form, and the values are scaled by u_τ^4/ν.
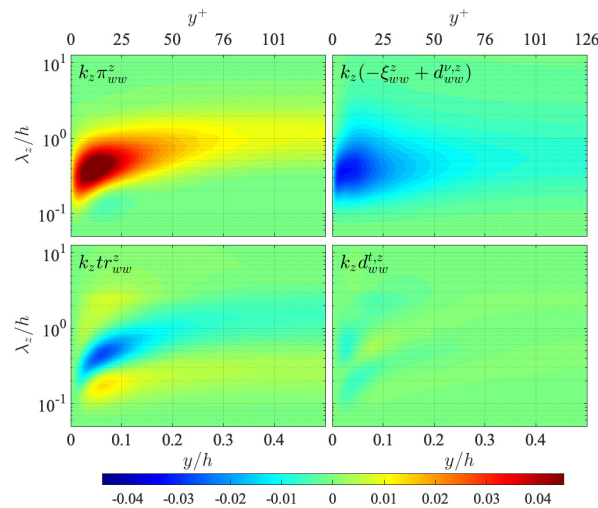

Figure A3. Distribution of terms in the transport equation of the spanwise turbulent energy spectrum E_{ww}^z, presented in the same manner as in Figure 12: (**top left**) pressure-strain energy redistribution π_{ww}^z; (**top right**) viscous terms $-\xi_{ww}^z + d_{ww}^{\nu,z}$; (**bottom left**) interscale transport tr_{ww}^z; (**bottom right**) turbulent diffusion $d_{ww}^{t,z}$. The terms are presented in the premultiplied form, and the values are scaled by u_τ^4/ν.
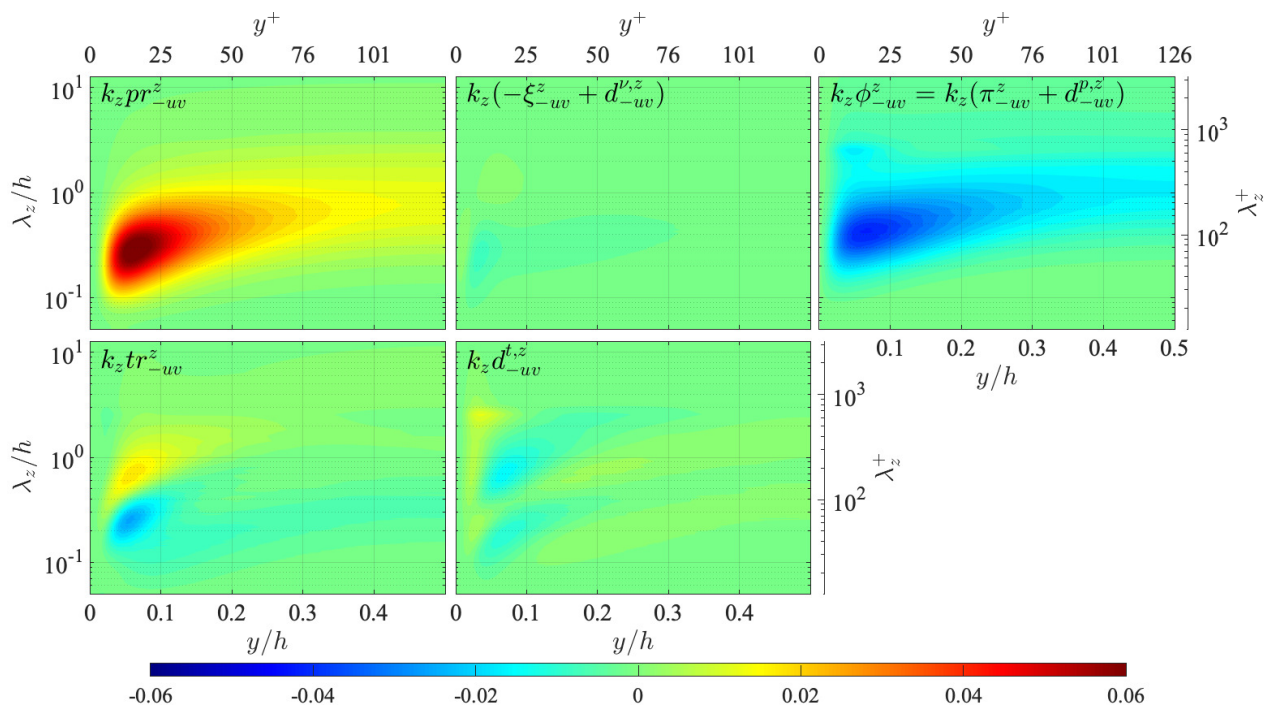
Figure A4. Distribution of terms in the transport equation of the Reynolds shear stress spectrum E^z_{-uv}, presented in the same manner as in Figure 12: (**top left**) production pr^z_{-uv}; (**top centre**) viscous terms $-\xi^z_{-uv} + d^{\nu,z}_{-uv}$; (**top right**) pressure term ϕ^z_{-uv}; (**bottom left**) interscale transport tr^z_{-uv}; (bottom centre) turbulent diffusion $d^{t,z}_{-uv}$. The terms are presented in the premultiplied form, and the values are scaled by u^4_τ/ν.

References

1. Kawata, T.; Alfredsson, P.H. Inverse Interscale Transport of the Reynolds shear stress in plane Couette turbulence. *Phys. Rev. Lett.* **2018**, *120*, 244501. [CrossRef]
2. Wang, W.; Pan, C.; Wang, J. Energy transfer structures associated with large-scale motions in a turbulent boundary layer. *J. Fluid Mech.* **2020**, *906*, A14. [CrossRef]
3. Doohan, P.; Wills, A.P.; Hwang, Y. Minimal multi-scale dynamics of near-wall turbulence. *J. Fluid Mech.* **2021**, *913*, A8. [CrossRef]
4. Kawata, T.; Tsukahara, T. Scale interactions in turbulent plane Couette flows in minimal domains. *J. Fluid Mech.* **2021**, *911*. [CrossRef]
5. Chan, C.; Schlatter, P.; Chin, R. Interscale transport mechanisms in turbulent boundary layers. *J. Fluid Mech.* **2021**, *921*, A13. [CrossRef]
6. Mizuno, Y. Spectra of energy transport in turbulent channel flows for moderate Reynolds numbers. *J. Fluid Mech.* **2016**, *805*, 171–187.
7. Lee, M.; Moser, R.D. Spectral analysis of the budget equation in turbulent channel flows at high Reynolds number. *J. Fluid Mech.* **2019**, *860*, 886–938. [CrossRef]
8. Wang, H.; Yang, Z.; Wu, T.; Wang, S. Coherent structures associated with interscale energy transfer in turbulent channel flows. *Phys. Rev. Fluids* **2021**, *6*, 104601. [CrossRef]
9. Cimarelli, A.; De Angelis, E.; Casciola, C.M. Paths of energy in turbulent channel flows. *J. Fluid Mech.* **2013**, *715*, 436–451. [CrossRef]
10. Cimarelli, A.; De Angelis, E.; Jiménez, J.; Casciola, C.M. Cascades and wall-normal fluxes in turbulent channel flows. *J. Fluid Mech.* **2016**, *796*, 417–436.
11. Chiarini, A.; Mauriello, M.; Gatti, D.; Quadrio, M. Ascending-descending and direct-inverse cascades of Reynolds stresses in turbulent Couette flow. *J. Fluid Mech.* **2021**, *930*, A9. [CrossRef]
12. Smits, A.; McKeon, B.; Marusic, I. High–Reynolds number wall turbulence. *Annu. Rev. Fluid Mech.* **2011**, *43*, 353–375. [CrossRef]
13. Cho, M.; Hwang, Y.; Choi, H. Scale interactions and spectral energy transfer in turbulent channel flow. *J. Fluid Mech.* **2018**, *854*, 474–504. [CrossRef]
14. Hamba, F. Turbulent energy density in scale space for inhomogeneous turbulence. *J. Fluid Mech.* **2018**, *842*, 532–553. [CrossRef]
15. Kawamura, H.; Ohsaka, K.; Abe, H.; Yamamoto, K. DNS of turbulent heat transfer in channel flow with low to medium-high Prandtl number fluid. *Int. J. Heat Fluid Flow* **1998**, *19*, 482–491. [CrossRef]
16. Kawamura, H.; Abe, H.; Matsuo, Y. DNS of turbulent heat transfer in channel flow with respect to Reynolds and Prandtl number effects. *Int. J. Heat Fluid Flow* **1999**, *20*, 196–207. [CrossRef]

17. Hane, S.; Tsukahara, T.; Iwamoto, K.; Kawamura, H. DNS of turbulent heat transfer in plane Couette flow. In Proceedings of the International Heat Transfer Conference, Sydney, Australia, 13–18 August 2006. [CrossRef]

18. Tsukahara, T.; Iwamoto, K.; Kawamura, H. On the large-scale structure of turbulent heat transfer in a plane Couette flow. *Therm. Sci. Eng.* **2007**, *15*, 151–161. (In Japanese)

19. Antonia, R.A.; Abe, H. Analogy between velocity and scalar fields in a turbulent channel flow. *J. Fluid Mech.* **2009**, *628*, 241–268. [CrossRef]

20. Abe, H.; Kawamura, H.; Toh, S.; Itano, T. Effect of the streamwise computational domain size on DNS of a turbulent channel flow at high Reynolds number. In *Advances in Turbulence XI*; Palma, J.M.L.M., Lopes, A.S., Eds.; Springer: Berlin/Heidelberg, Germany, 2007; pp. 233–235.

21. Alcántara-Ávila, F.; Hoyas, S.; Pérez-Quiles, M.J. DNS of thermal channel flow up to $Re_\tau = 2000$ for medium to low Prandtl numbers. *Int. J. Heat Mss Transf.* **2018**, *127*, 349–361. [CrossRef]

22. Alcántara-Ávila, F.; Gandía-Barberá, S.; Hoyas, S. Evidences of persisting thermal structures in Couette flows. *Int. J. Heat Fluid Flow* **2019**, *76*, 287–295. [CrossRef]

23. Alcántara-Ávila, F.; Hoyas, S.; Jezabel Pérez-Quiles, M. Direct numerical simulation of thermal channel flow for $Re_\tau = 5000$ and $Pr = 0.71$. *J. Fluid Mech.* **2021**, *916*, A29. [CrossRef]

24. Alcántara-Ávila, F.; Hoyas, S. Direct numerical simulation of thermal channel flow for medium–high Prandtl numbers up to $Re_\tau = 2000$. *Int. J. Heat Mss Transf.* **2021**, *176*, 1214112. [CrossRef]

25. Komminaho, J.; Lundbladh, A.; Johansson, A.V. Very large structures in plane turbulent Couette flow. *J. Fluid Mech.* **1996**, *320*, 259–285. [CrossRef]

26. Kitoh, O.; Nakabayashi, K.; Nishimura, F. Experimental study on mean velocity and turbulence characteristics of plane Couette flow: Low-Reynolds-number effects and large longitudinal vortical structure. *J. Fluid Mech.* **2005**, *539*, 199–227. [CrossRef]

27. Tsukahara, T.; Kawamura, H.; Shingai, K. DNS of turbulent Couette flow with emphasis on the large-scale structure in the core region. *J. Turbul.* **2006**, *7*, N19. [CrossRef]

28. Kitoh, O.; Umeki, M. Experimental study on large-scale streak structure in the core region of turbulent plane Couette flow. *Phys. Fluids* **2008**, *20*, 025107. [CrossRef]

29. Avsarkisov, V.; Hoyas, S.; Oberlack, M.; García-Galache, J.P. Turbulent plane Couette flow at moderately high Reynolds number. *J. Fluid Mech.* **2015**, *751*, R1. [CrossRef]

30. Orlandi, P.; Bernardini, M.; Pirozzoli, S. Poiseuille and Couette flows in the transitional and fully turbulent regime. *J. Fluid Mech.* **2015**, *770*, 424–441. [CrossRef]

31. Lee, M.; Moser, R.D. Extreme-scale motions in turbulent plane Couette flows. *J. Fluid Mech.* **2018**, *842*, 128–145. [CrossRef]

32. Kawata, T.; Tsukahara, T. Spectral analysis on dissimilarity between the turbulent heat and momentum transport in plane Couette turbulence. *Phys. Fluids* **2022**. [CrossRef]

33. Kawata, T.; Alfredsson, P.H. Scale interactions in turbulent rotating planar Couette flow: Insight through the Reynolds stress transport. *J. Fluid Mech.* **2019**, *879*, 255–295. [CrossRef]

34. Toh, S.; Itano, T. Interaction between a large-scale structure and near-wall structures in channel flow. *J. Fluid Mech.* **2005**, *524*, 249–262. [CrossRef]